THE UNIVERSITY OF OKLAHOMA

GRADUATE COLLEGE

AN IMPROVED METHOD FOR MEASURING OPTICAL EXCITATION FUNCTIONS

A DISSERTATION

SUBMITTED TO THE GRADUATE FACULTY

in partial fulfillment of the requirements for the

degree of

DOCTOR OF PHILOSOPHY

BY

CHARLES J. BRONCO

Norman, Oklahoma

1959

AN IMPROVED METHOD FOR MEASURING

OPTICAL EXCITATION FUNCTIONS

APPROVED BY

R. G. Fowler

A. van Engel

Robert M. St. John

Colin H. Flint

Arthur Bernhart

DISSERTATION COMMITTEE

ACKNOWLEDGMENTS

The author wishes to express his appreciation and thanks to Dr. R.G. Fowler, who directed the research, for his assistance and advice throughout the course of the work.

The author would also like to express his gratitude to:

Dr. R.M. St.John, who co-directed the research project, for his valuable assistance in performing the research;

Dr. A.H. Von Engel, acting in the capacity of advisor, for his constructive criticism, active interest in the research and able advice;

Dr. P.F. Little for advice on construction of the apparatus;

the Graduate Faculty for their cooperation and lending of equipment;

Robert Smay, Tom Brown and Fred Fajen for aid in constructing the apparatus;

Mr. J.C. Hood for performing the machine work on the parts;

Mr. R.W. Lawrence for successfully performing the difficult glass work;

Mrs. Raymond Adair for typing the thesis.

This work has been done as part of a project sponsored by the Air Force Office of Scientific Research.

TABLE OF CONTENTS

LIST OF TABLES

LIST OF ILLUSTRATIONS

AN IMPROVED METHOD FOR MEASURING OPTICAL EXCITATION FUNCTIONS

CHAPTER I

INTRODUCTION

The probability of an electron of a given velocity striking an atom of a gas in the ground state and raising it into a particular excited state is proportional to the excitation cross-section for that excited state. The dependence of the excitation cross-section on the electron energy is known as the excitation function.

When the energy of the incoming electron exceeds the threshold for excitation, there is a finite probability to raise the atoms into the excited state. If the electron has an energy equal to or less than that of the excited state, the probability of excitation is zero. When the atom undergoes a transition from the excited state to a lower state, a photon is emitted with an energy equal to the difference in the two atomic energy levels involved. Hence if one could measure the absolute intensity of the light emitted in a given atomic transition, the cross-sections for excitation to its energy level could be determined.

The optical method for measuring excitation cross-sections consists of shooting a known number of electrons per second through a gas

at a known pressure and measuring the absolute intensity of the light emitted in a given atomic transition.

Electron collisions can be subdivided into elastic collisions, in which the total kinetic energy of the colliding system is conserved; and inelastic collisions, in which part of the kinetic energy of the colliding system is transformed into internal potential energy of at least one member of the colliding system. Inelastic electron collisions can be further subdivided into inelastic collisions of the first kind, in which the total kinetic energy of the colliding system is reduced by the collision; and inelastic collisions of the second kind, in which the internal potential energy of at least one member of the colliding system is reduced by the collision.

Electrical Method of Measuring Excitation Cross-Sections

Besides the optical method for studying excitation cross-sections, the electrical method has been used at small electron energies, (from the lowest threshold to 35 volts). Maier-Leibnitz (13) applied this method to investigate excitation in He, Ne, and A. It is based on an analysis of the energy distributions of electrons moving through a gas which possess sufficient energy to excite the gas.

As the electron energies increase it becomes more difficult to resolve differences in current collected, so that the electrical method is most efficient at low electron velocities. The optical method, however, becomes better with increasing electron energies so that the two methods complement each other in this respect. They are not, however, in perfect agreement. For some states there is no overlap in the parts of the curve measured by the two methods.

Previous Optical Experiments on Excitation

All of the following optical experiments utilized photographic methods of measuring light intensity. Hughes and Lowe (10) used photometric methods which were incapable of great accuracy and did not have linearity between intensity and current or intensity and pressure. Their results were not strikingly different from Lees' (12) results, who did have linearity between intensity and current.

Peteri and Elenbaas (18) obtained extremely different curves than those obtained by Hughes and Lowe. Elenbaas found that all lines show a slight maximum at about 60 volts. Elenbaas also did not get linearity between current and intensity or pressure and intensity.

Hanle (8) also did not have the above mentioned linearity. Michels (15) obtained this linearity and observed a second maxima at about 80 volts for all lines. Michels moreover used a nonhomogeneous beam of electrons, only 90 per cent lying within a 10 volt range.

Lees (12) used an oxide coated cathode and an electron gun which had no velocity selection; by use of a stopping power experiment he concluded that 90 per cent of the electrons were in a 3.5 volt range. He used a helium pressure of 4×10^{-2}mm and an electron current of 0.8 milliamperes. Lees observed some of the lines (such as the 5016A of helium) on an intensity-pressure plot seemed to intersect the pressure axis at a finite pressure. There seemed to be no light emitted by the line 5016A when the gas was at a pressure of 10^{-2}mm or lower. He also noticed that light was coming from outside the beam for these lines. Lees' results compare favorably with Thieme's (21) results for some lines and disagree by orders of magnitude for others. It is worth noting that both disagree

with any acceptable theory (14).

CHAPTER II

THEORY

Theoretical calculation of the Excitation Cross-Section by Born's Approximation Method.

Let the incident electron be designated by the suffix 1 and the outer electron of the helium atom by the suffix 2. If the inner atomic electron and the helium nucleus is regarded as a screened potential of charge +1, then the wave equation for the incident electron and helium atom is given by;

$$\left[\nabla_1^2 + \nabla_2^2 + \frac{2M}{\hbar^2}\left(E + \frac{e^2}{r_1} + \frac{e^2}{r_2} - \frac{e^2}{r_{12}}\right)\right]\Psi = 0$$

where the nucleus is taken as the origin and,

r_1 = incident electron distance from origin

r_2 = outer electron distance from origin.

Following Massey (14) Ψ is expanded in terms of the orthogonal set of eigenfunctions $\psi_n(r_2)$ in the form,

$$\Psi = \Sigma \psi_n(r_2)\, F_n(r_1).$$

Substituting this into the wave equation gives,

$$\Sigma_n \psi_n(r_2)\left[\nabla_1^2 + k_n^2\right] F_n(r_1) = \frac{2me^2}{\hbar^2}\left(\frac{1}{r_{12}} - \frac{1}{r_1}\right)\Psi.$$

Multiplying both sides by $\Psi_n^*(r_2)$ and integrating over dr_2 gives,

$$(\nabla_1^2 + k_n^2)\ F_n(r_1) = \frac{2me^2}{\hbar^2} \int \Psi_n^* \left(\frac{1}{r_{12}} - \frac{1}{r_1}\right) \Psi\, dr_2$$

or,

$$(\nabla_1^2 + k_n^2)\ F_n(r_1) = \sum_m U_{nm}\, F_m$$

where,

$$U_{nm} = \frac{2me^2}{\hbar^2} \int \Psi_n^* \left(\frac{1}{r_{12}} - \frac{1}{r_1}\right) \Psi_m\, dr_2.$$

This coupled set of simultaneous integro-differential equations can be solved for the $F_n(r_1)$. If the incident electrons are represented as a plane wave, then the $F_n(r_1)$ are made up of the incident plane wave and spherical scattered waves about the atom of the form,

$$F_n(r_1) = e^{ik_o(\bar{n}_o \cdot \bar{r}_1)} + r^{-1} e^{ik_n r_n} f_n(\theta, \varphi).$$

The differential cross-sections are given by

$$k_n/k \left[f_n(\theta, \varphi)\right]^2.$$

$F_o(r_1)$ represents the incident plane wave and the elastically scattered wave. The $F_n(r_1)$ for $n \neq o$ represent the scattered wave after exciting the atom to the state n.

It is impossible to solve these equations exactly. If the perturbation by interaction is treated as small, the set of simultaneous differential equations can be reduced to

$$(\nabla_1^2 + k_n^2)\ F_n(r_1) = U_{no}\, e^{ik_o n_o \cdot r_1}.$$

This is called the Born (3) approximation. A more complete discussion of the conditions for realizing the Born Approximation can be found in

Mott and Massey (24). The solution of these equations can be found in Schiff (25) and is arrived at by the use of Green's theorem. This solution is given by,

$$F_o(r_1) = e^{ik_o \bar{n}_o \cdot \bar{r}} - \frac{1}{4\pi} \int \mathcal{U}_{oo}(r') e^{ik_o n_o r'} \frac{e^{ik_o |r-r'|}}{|r-r'|} dr', \quad n=0$$

$$F_n(r_1) = -\frac{1}{4\pi} \int \mathcal{U}_{no}(r') e^{ik_o n_o \cdot r'} \frac{e^{ik_n |r-r'|}}{|r-r'|} dr', \quad n \neq 0$$

If the above solutions are taken to represent the incident electron instead of the plane wave used to get these solutions, then the solution to the Born equation gives a better approximation to the actual case. This is called the second Born approximation. This is used by Rothenstein to calculate the cross-section for the $1^1S \rightarrow 2^1P$ transition in helium.

Electron Exchange

The above treatment of the electron scattering process does not account for the case when the incident electron is captured and the atomic electron ejected.

Interchanging the electrons results in a Born equation with $G_n(r_2)$ replacing $F_n(r_1)$ and $\psi n(r_2)$ replaced by $\varphi n(r_1)$. The solutions are identical with the above substitutions, with,

$$G_n(r_2) \sim r_2^{-1} e^{ik_n r} g_n(\theta, \varphi).$$

Oppenheimer (16) showed that, for hydrogen, the cross section for a given inelastic collision involving excitation of the n-th state is given by,

$$I_n(\theta, \varphi) = \frac{1}{4} I_n^+ + \frac{3}{4} I_n^-$$

where,

$$I_n^+ = |f_n + g_n|^2 \ (k_n/k_o)$$

$$I_n^- = |f_n - g_n|^2 \ (k_n/k_o).$$

Agreement of Experimental Results and Born's Approximation

Figure 1 shows that the experiment of Thieme's and theory agree well at large energies. As the energy becomes smaller, theory overestimates the magnitude of the cross-section. Theory also reaches a maximum at lower energies than results from experiment. It is estimated that Born's approximation starts overestimating the cross-section at 7 to $10E_o$, where E_o is threshold energy. Born's second approximation seems to cause the overestimation to be less at lower energies and the maximum to occur at a higher energy.

Energy Levels of Helium

The energy levels of the helium atom are given in Figure 3. The 5016A line investigated by the method of this thesis is indicated by a dotted line as is the corresponding triplet line, 3888A.

Polarization of the Helium Radiation

The radiation from the helium gas, (upon being struck by electrons), exhibits a polarization effect, determined by the direction of the exciting electron beam.

The percentage polarization A is defined by,

$$A = 100 \ \frac{I_{\parallel} - I_{\perp}}{I_{\parallel} + I_{\perp}}$$

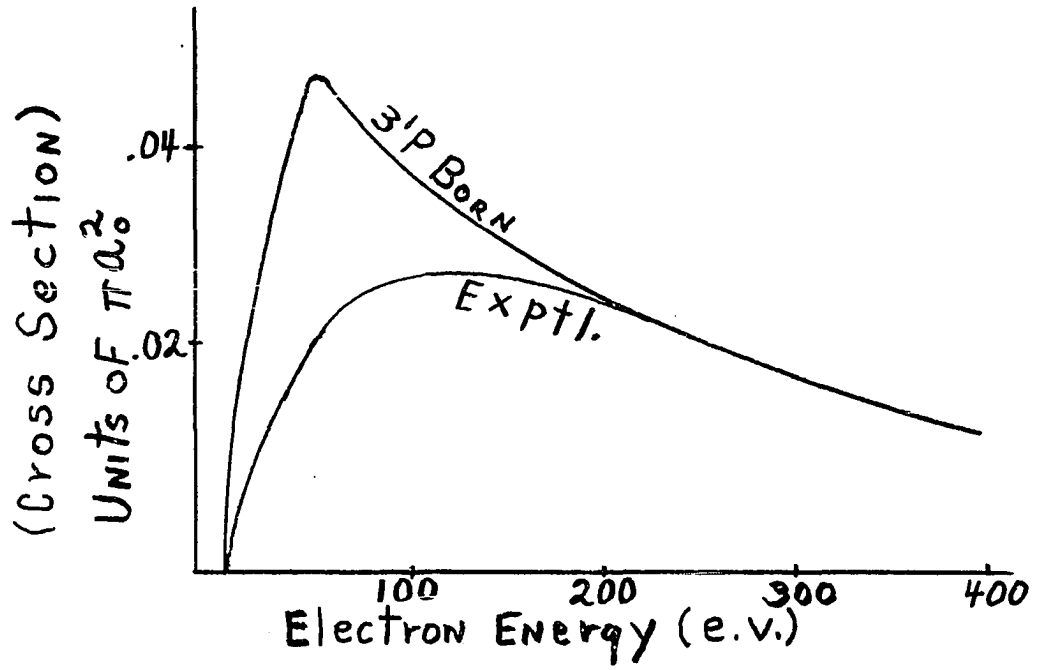

Figure 1. Comparison of Theoretical with Average Experimental Excitation Function

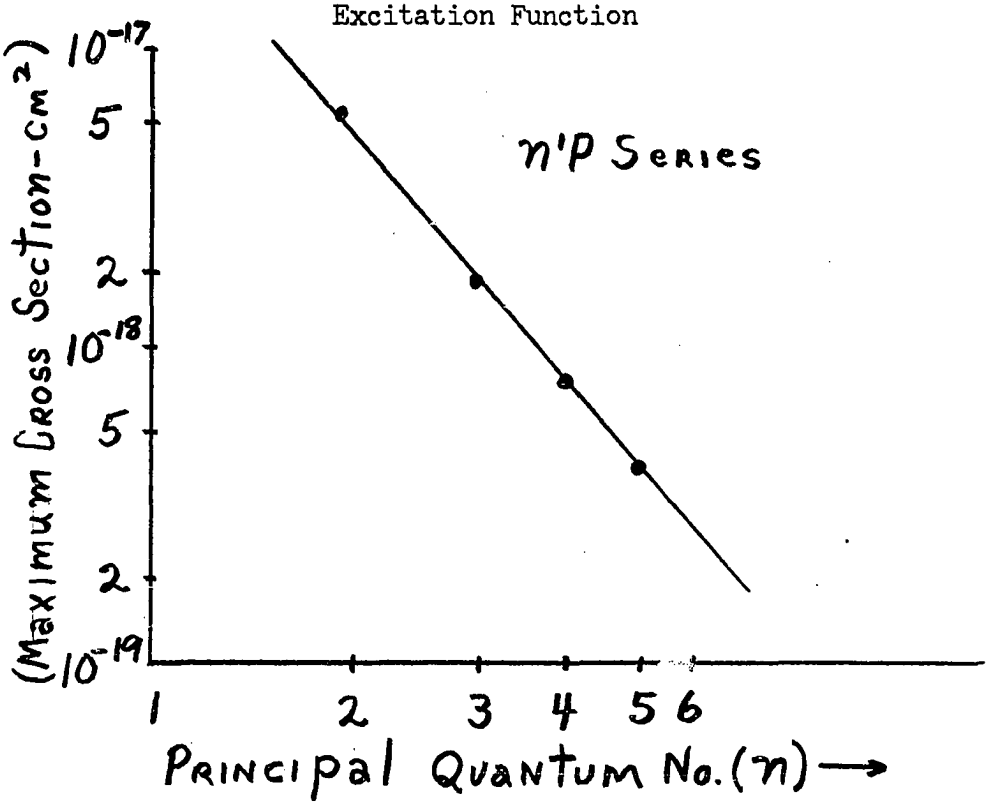

Figure 2. Theoretical Prediction of decrease of Q_j max. with increasing n.

where:

$I_{\parallel}$ = Intensity of the emitted light polarized parallel to direction of the electron beam,

$I_{\perp}$ = Intensity of the emitted light polarized perpendicular to the direction of the electron beam.

The polarization seems to be zero at the excitation potential but increases sharply at low velocities and passes through a maximum a few volts above the excitation potential (20).

Transitions from singlet P to S levels seem to have a maximum polarization of less than 10 per cent. In calculating the excitation cross-sections, from data obtained by viewing the electron beam at a fixed angle, a percentage error is introduced if one considers the photons given off to have a spherical distribution. This would vary with the exciting voltage but would be less than 5 per cent for lines arising from transitions from P to S levels.

Population Balance of Excited States

The population of atoms in an excited state N_j may be added to by direct excitation to this level from the ground state by an electron beam or by decay from higher states. Atoms may leave it by decay to lower levels.

If we assume further that there are no collisions between electrons and excited atoms nor excited states and normal gas atoms then,

$$dN_j/dt = -A_jN_j + NQ_v N_e + \Sigma A_{ij}N_i$$

where:

A_{ij} = Probability per second of radiative transition from ith to jth state.

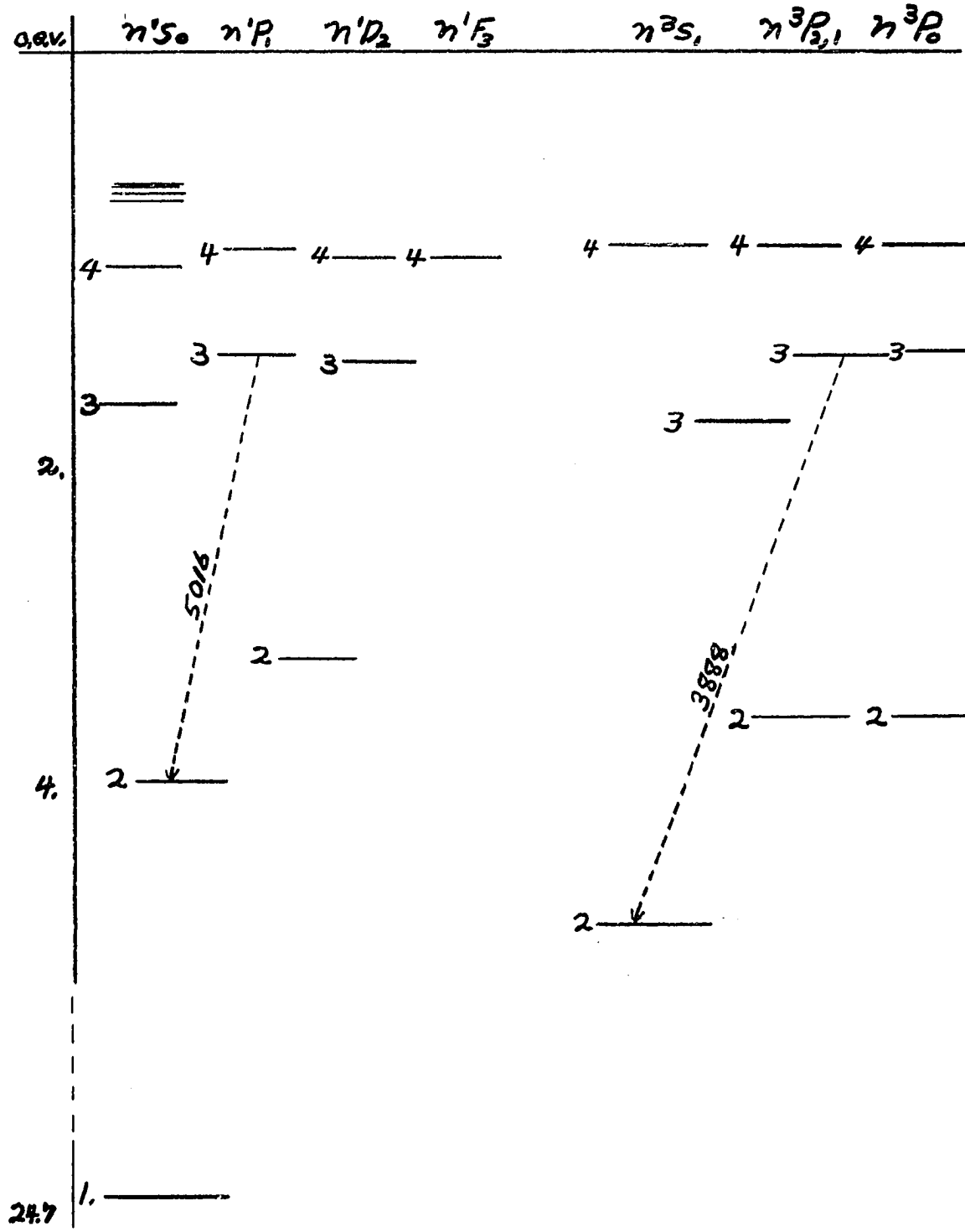

Figure 3. Helium Energy Level Diagram

$A_j = \sum_k A_{jk}$ where k is the suffix for levels lower than j.

Q_j = cross-section for excitation to the jth level

v = electron velocity

Ne,N = Number of electrons and gas atoms per cubic centimeter.

In equilibrium,

$$N_j = (NQ_j v N_e + \sum A_{ij} N_i) / A_j .$$

The total number of quanta emitted per unit length of the electron beam corresponding to the transition $j \rightarrow K$ is,

$$J_{jk} = A_{jk} N_j S$$

where:

S = cross-sectional area of beam.

Since,

$$i = vSeN_e$$

we get,

$$J_{jk} = A_{jk} / A_j \left\{ NQ_j \frac{i}{e} + \sum_i J_{ij} \right\} .$$

It follows that if measurements are made of the absolute intensities of the radiation emitted in transitions both to and from the jth state of the atom, then the cross-section Q_j may be obtained from the above equation, provided the pressure is low enough to prevent any secondary effects (22), such as, resonance radiation, collisions of the second kind, etc.

Resonance Radiation

Resonance radiation effects usually arise when the particular jth state has an optically allowed chance of going directly to the ground state. Since a majority of the atoms are in the ground state, the radiation from the level j to the ground state has a good chance of re-

exciting other ground state atoms into the level j. There is a chance that the re-excited level j will re-radiate to the ground state by a combination of other transitions instead of $j \rightarrow k$, where k is the ground state.

Figure 4 shows the relationship of the intensity for the $3^1P \rightarrow 2^1S$ transition and the pressure, expected from considering only the theoretical behavior of the resonance radiation (17). The pressure dependence actually measured may differ from this due to other secondary phenomena. Massey (14) says that the discrepancy for the 3^1P excitation cannot be wholly ascribed to trapping of resonance radiation.

Phelps' theory (17) states that at the helium pressures commonly used (10^{-3} to 10^{-1}mm of Hg.) the observed visible radiation may easily be a factor of ten greater than that expected when imprisonment effects are neglected.

Data reported in this thesis was obtained at gas pressures low enough to avoid resonance radiation effects.

The above arguments show resonance radiation effects (as do other pressure-dependent secondary phenomena) disappear when the line intensity being measured becomes a linear function of the pressure.

Rather than depend on theoretical calculations for the pressure at which resonance radiation effects disappear, a line intensity versus pressure graph was made.

Figure 27, Chapter VII, shows the pressure dependence experimentally measured by the methods of this thesis. The pressure selected to be used in this experiment was taken from the lower linear region of this curve.

Cascading From the 3^1P Level To Lower Levels

For the level 3^1P, investigated in this thesis, there are three optically allowed ways of relaxing to the ground state: $3^1P \rightarrow 3^1S$ $2^1P \rightarrow 1^1S$; $3^1P \rightarrow 2^1S$ followed by a non radiative wall collision; or directly as $3^1P \rightarrow 1^1S$. The transition $3^1P \rightarrow 1^1S$ is in the far ultra-violet and can excite other atoms from the ground state to the 3^1P level. The re-excited atom, being in the 3^1P state, can again either relax to the 2^1S or 1^1S level. This has the effect of enhancing the $3^1P \rightarrow 2^1S$ radiation as viewed outside the gas, at the expense of the $3^1P \rightarrow 1^1S$ radiation. When the gas pressure is low enough so that the mean free path for photon diffusion is large in comparison with the dimensions of the container, there is a constant ratio of the intensity of the two lines for any further reduction of the pressure. The ratio is determined by their relative transition probabilities.

This ratio can be measured experimentally by measuring the absolute intensity of both lines at sufficiently low pressures. Since the line $3^1P \rightarrow 1^1S$ is in the far ultra-violet, its absolute intensity is difficult to measure experimentally.

A theoretical estimation of the ratio can be attained by using the ratio of their transition probabilities. An experimental check can be obtained by experimentally measuring the half lives of the levels (9). The reciprocal of the half-lives are the transition probabilities.

The transition probabilities, A_{jk}, have been computed theoretically for the levels of interest to this thesis by Hylleraas, Bates and Damgaard (2), and by Goldberg. The values for these A_{jk}'s also can be calculated from data given in tables by Landolt-Bornstein (Vol. 1, Part 1,

1950). Using these optical transition probabilities, Hylleraas (11) found that,

$$\frac{A\,(3^1P \rightarrow 2^1S)}{A\,(3^1P \rightarrow 3^1S)\quad A\,(3^1P \rightarrow 2^1S)\quad A\,(3^1P \rightarrow 1^1S)} \approx \frac{1}{40.2}$$

Cascading to the 3^1P State From Upper Levels

The excitation cross section for a given series at a particular electron energy varies inversely as the cube of n, the principal quantum number. This is shown in Figure 2 which summarizes theory and experimental data regarding this point. From this relationship, it can be seen that the contribution to the 3^1P states due to cascading into the level from above diminishes progressively as the contributor's principal quantum number increases. This is because fewer atoms are excited into these states compared to the lower states.

Due to this rule and selection rules, it follows that the principal contributors to the 3^1P state as a result of cascading from above are the 4^1S and 4^1D states (See Figure 6).

After being excited the 4^1S state can lose its excitation by $4^1S \rightarrow 3^1P$ or by $4^1S \rightarrow 2^1P$ transitions. The transition probabilities are approximately the same and about half of the 4^1S states will decay into 3^1P states.

The excitation cross-section ratio of $4^1S/3^1P$ at 60 volts is given by Theime (21) as 11.4/72. When this is multiplied by the branching factor for the 4^1S state, this gives the fraction of the 3^1P states contributed by cascade from the 4^1S state.

This is approximately 8 per cent of the 3^1P cross-section measured by Thieme at 60 volts. It falls to 5 per cent at 100 volts.

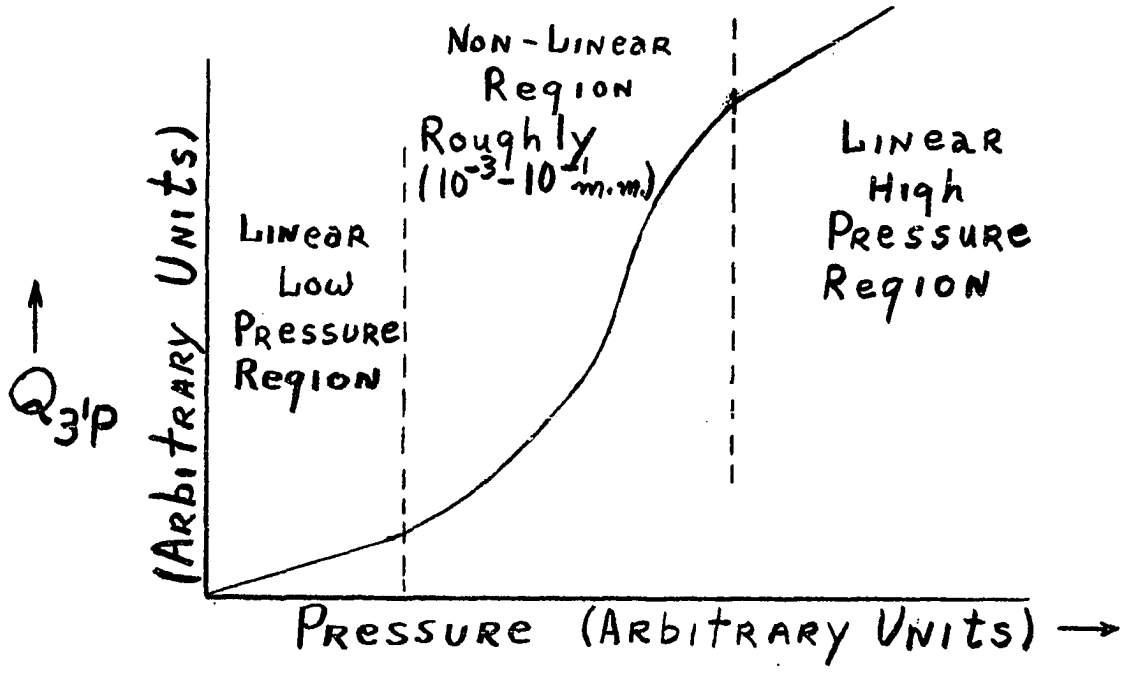

Figure 4. Expected Pressure dependence due to Resonance Radiation

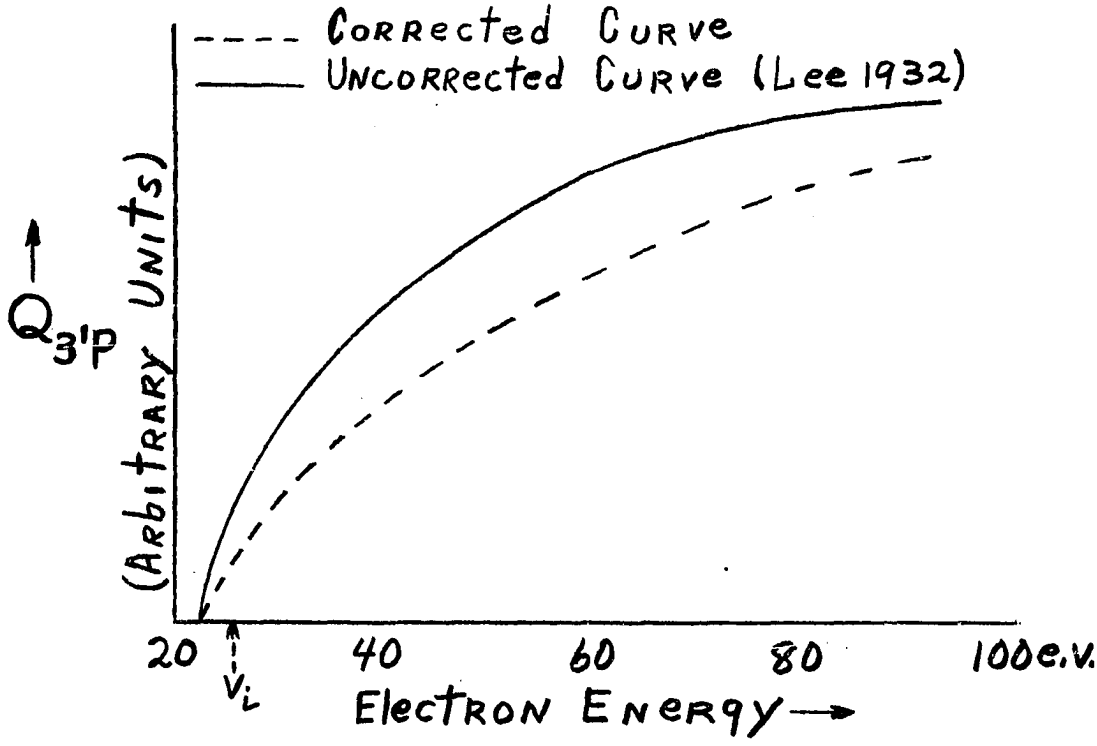

Figure 5. Correction For Cascading From Above

The contribution from the 4^1D levels is slightly less percentage-wise than the 4^1S contribution.

In Figure 2 of the Westinghouse (7) report a curve is given for the correction of cascade to the 4^1P level. This correction is very nearly the same for the 3^1P level, due to the fact that we have the same situation except the principal quantum number is raised by one for all levels.

The correction is larger for lower voltages because the 4^1S and 4^1D levels peak before the 3^1P as estimated from Lees' and Theime's data.

Figure 6 shows how the level 3^1P is populated. The wavy lines represent photo-relaxation to lower states. The solid lines represent direct electron collision excitation from the ground state.

Figure 5 gives the correction to be applied to the cross-section for excitation from the ground state to the 3^1P state due to cascading from states with $N \geq 4$ (7).

To correct for cascading from above, the ideal way would be to measure the cross-sections experimentally for the 4^1S and 4^1D as well as for the 3^1P state. If the corrected cross-sections for the 4^1S and 4^1D states were known, the corrected cross-section for the 3^1P state could be calculated.

The absolute magnitude of the cross-sections for the 4^1S and 4^1D states measured by Lees may not agree with those measured on the experimental equipment of this thesis. For this reason the cascading from above has been treated as a percentage-wise negligible quantity, especially at voltages greater than 50 volts. The 3^1P function appearing in Chapter VIII is thus uncorrected for the small error resulting from

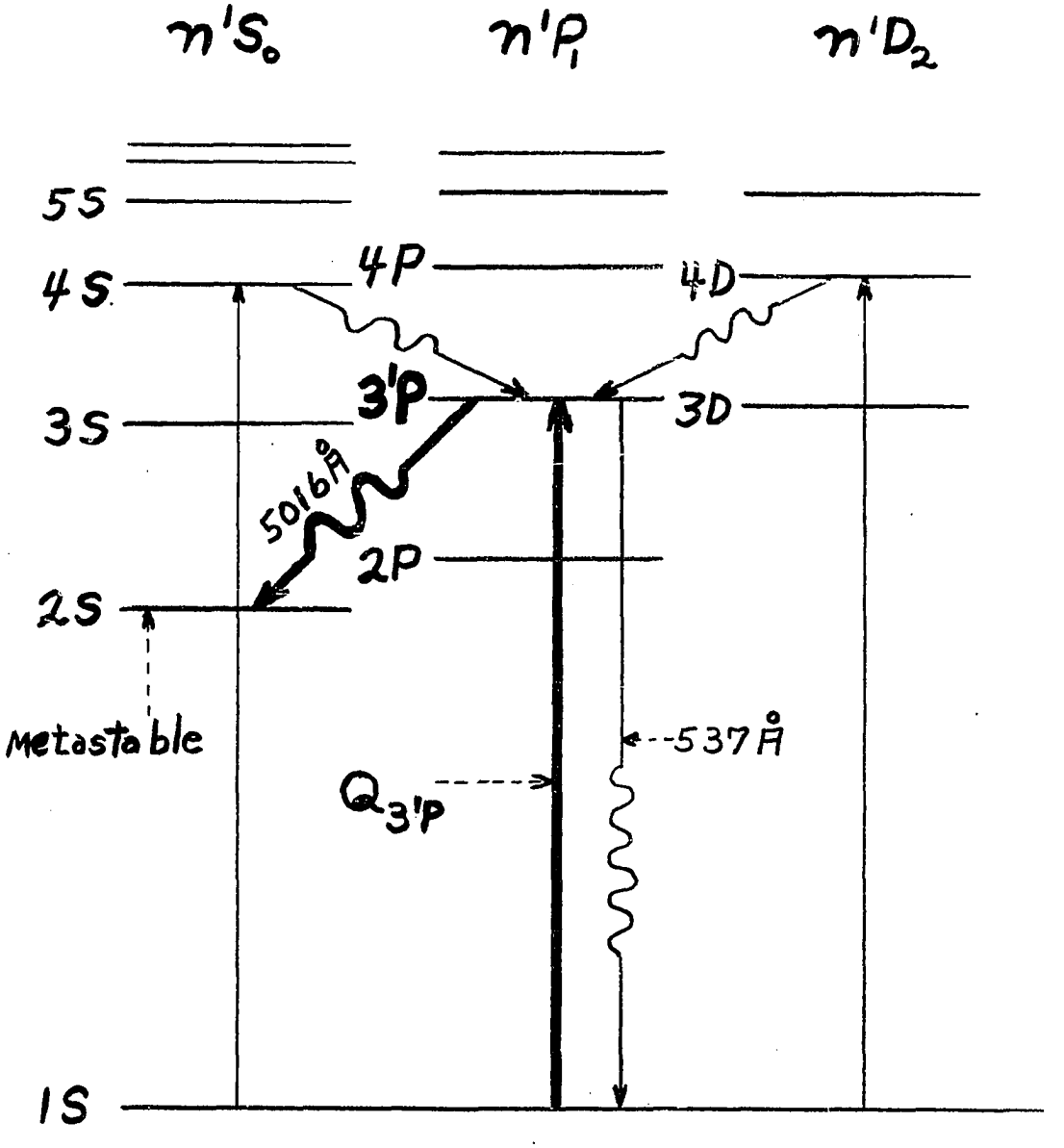

Figure 6. Population Balance of the 3^1P State

cascading from above.

In experiments such as those of Lees (12) and Theime (21), it is thought that levels were populated to a considerable extent by processes other than direct impact excitation. Reactions such as,

$$1^1S + 4^1P \rightarrow 4^3D + 1^1S$$

were thought to occur at a rate sufficient to mask direct impact production of 4^3D atoms.

This type of process is dependent upon the half-lives of the colliding excited state (4^1P state for the above mentioned case) as well as the pressure and the dimensions of the containing vessel.

Relationship of Half-Life and Pressure for Collision Excitation-Transfer Processes.

Let N be the total number of atoms per cubic centimeter, N_i the number of atoms in the ith excited state, N_o the number in the ground state, Q_{ij} the excitation cross-section from the jth to the ith state and t_{ij} the half-life of the ith state before going to the jth state. Then the number of atoms excited to the ith state per second per centimeter of path length by an electron beam of strength n is given by,

$$N_o Q_{ij} n_o$$

where n_o is the number of electrons passing a point in the beam per second.

The mean free path for atomic collisions is given by,

$$\frac{1}{\sqrt{2}\pi r_o^2 N}$$

where r_o is the collision radius for the atoms. For helium atoms this expression is given roughly by $10^{16}/N$. The radius r_o is larger for an excited atom. The collision radius for excited atoms was estimated by Lees to be 10^{-7}cm, which would give $2 \times 10^{13}/N$ for the mean free path for excited helium atoms.

At standard temperature the velocity of the helium atoms is of the order of 10^5cm/sec.

The number of excited atoms existing at any one time per centimeter of beam path is,

$$N_i = NQ_{ij}n_o t_{ij}.$$

The fraction of the total number of atoms which are in an excited state during the time interval t_{ij} is given by,

$$NQ_{ij}\, n_o\, t_{ij}/N.$$

The number of excited-atom--neutral-atom collisions in t_{ij} seconds is given by,

$$(N\, Q_{ij}\, n_o\, t_{ij}/N)\ \ (10^5 N/2.10^{13}/N)\, t_{ij}$$

$$= n_o\, Q_{ij}\, N^2\, t_{ij}^2 \,/\, 2.10^8 = N^*$$

The ratio of the excited atoms having collisions with neutral atoms to the number of excited atoms is,

$$N^*/N_i^3 = (Q_{ij}\, n_o\, N^2\, t_{ij}^2 \,/\, 2.10^8)\ (N\, Q_{ij}\, t_{ij}\, n_o)$$

$$= N\, t_{ij}/\, 2.10^8.$$

This means that as long as

$$N t_{ij} < 2 \times 10^{6}$$

collisions of the second kind effect less than one per cent of the excited atoms, which in turn means that at 10^{-2}mm of pressure or less, states with half-lives of 10^{-8} seconds or less do not lose an appreciable amount of their excited energy to collisions of the second kind.

For meta-stable states with half-lives greater than 10^{-5} second, collisions of the second kind would be the predominating mechanism even at pressures below 10^{-3}mm. It has been assumed that collisions with the walls of the container are collisions of the second kind.

From the above treatment it seems that in a helium gas, where, with the exception of meta-stable states, the half lives are not considered larger than 10^{-5} to 10^{-6} seconds, the influence of collisions of the second kind should be negligible below 10^{-3}mm Hg.

CHAPTER III

EXPERIMENTAL METHODS

Purpose of Experiment

The experimental objectives were:

(a) To better establish the absolute value of excitation cross-sections and their dependency on energy.

(b) To establish an optical method sensitive enough to study the excitation functions at pressures, (10^{-4}mm), two orders of magnitude below that of all previous experiments on excitation, (10^{-2}mm). This was important as it was established that secondary phenomena had made previous measurements pressure dependent.

(c) To attain a tenfold better energy resolution than previously. There exists some theoretical evidence (7) that there are resonance peaks on the excitation functions for some lines. To resolve these would require a resolution of 0.1 volts.

(d) To insure a cleaner gas while the measurements are being made by the use of newly developed high vacuum techniques and equipment.

(e) To perform a careful calibration to make the measurements absolute.

Means Used to Obtain Experimental Goals

It was decided to use velocity selection for the electrons since

no cathode emits electrons in a narrow enough energy range. Ramsauer (19) type velocity selection, consisting of a magnetic field and defining holes was chosen. The electron paths are bent in circles of various sizes depending upon their energy. For a given magnetic field electrons with smaller energies will have paths of smaller radii. Baffles with holes define a circle of a known radius corresponding to a certain electron energy. The resolution of this device will be given later in this chapter.

Cathode

It is best to use velocity selection in conjunction with a cathode which yields the electrons in as narrow an energy band as possible in order to avoid selecting out too much of the beam current. Barium impregnated tungsten cathodes of the types developed by the North American Phillips Company were used.

Light Sensitive Measuring Device

In order to operate at the desired pressures, very small light fluxes had to be measured. A photon counting technique was adopted (5). Its essential parts are shown in the block diagram of Figure 7.

Light coming from the excited atoms is focused on a filter system where photons of a single wave length are selected and passed on to the photomultiplier to be counted.

The photomultiplier is an EMI 6256B-type tube with 13 stages. This is an advantage because one needs less voltage per stage to amplify internally a single electron event enough that a linear amplifier could in turn amplify it to the threshold of a scalar. Less voltage per stage

is important because dark current increases as the voltage per stage increases.

Since the dark current is also proportional to the tube temperature, refrigeration of the tube to liquid air temperatures was required. A description of the refrigerator will be given in Chapter IV.

The photomultiplier voltage was supplied by batteries. In order to couple the photomultiplier output to the scalar and retain a microsecond rise time, a cathode-follower coupling stage was used.

Ultra High Vacuum System

An Alpert-type ultra-high vacuum system was built to insure purity of the working gas. This consisted of a 3-stage oil diffusion pump, copper traps, all metal valves and an ionization pump and gauge.

A special bake-out oven capable of attaining 550° C. was constructed. The system was baked out for four hours at 400° C.

The oil pump took the clean system to 10^{-7}mm. The valves were then closed and the ion pump reduced the pressure to less than 10^{-10}mm. A special vacuum-tube electrometer was constructed to measure the positive ion current (10^{-7}ma) of the ion gauge at the lowest pressure.

The pressure measuring apparatus consisted of a thermocouple gauge to measure pressures above 10^{-3}mm and an ion gauge to measure pressures below 10^{-3}mm.

Separate Vacuum System for Photomultiplier

A separate vacuum system was built for the photomultiplier and its refrigerator. The photomultiplier and its input resistors were mounted in vacuum and kept at a pressure of less 10^{-5}mm whenever the

high voltage was applied.

Electron Beam Energy Resolution

A derivation of the theoretical electron energy resolution of the system of baffles for the 180 degree tube shown in Figure 8 and a magnetic field perpendicular to the plane of the paper is given below.

In Figure 8,

$$\Delta R = R_2 - R_1$$

and,

$$X_1 = R_1 - \frac{C}{2}$$

$$Y_1 = R_1 + S/2$$

where:

S = entrance and exit slit width.

C = center slit opening.

Looking at the sagitta of the larger circle of radius R_2,

$$Y_1^2 = (2R_2 - X_1)\, X_1.$$

Substituting the values for X_1 and Y_1 given above, gives the relation,

$$(R_1 + \frac{S}{2})^2 = \left[2R_2 - (R_1 - \frac{C}{2})\right] \quad (R_1 - \frac{C}{2}).$$

This is a relation between R_2 and S, C and R_1. From it R_2 can be calculated and knowing R_2, ΔR can be calculated. From the relation,

$$\frac{\Delta E}{E} \qquad \frac{2\Delta R}{R}$$

the energy band ΔE of the electrons which will get through the slits

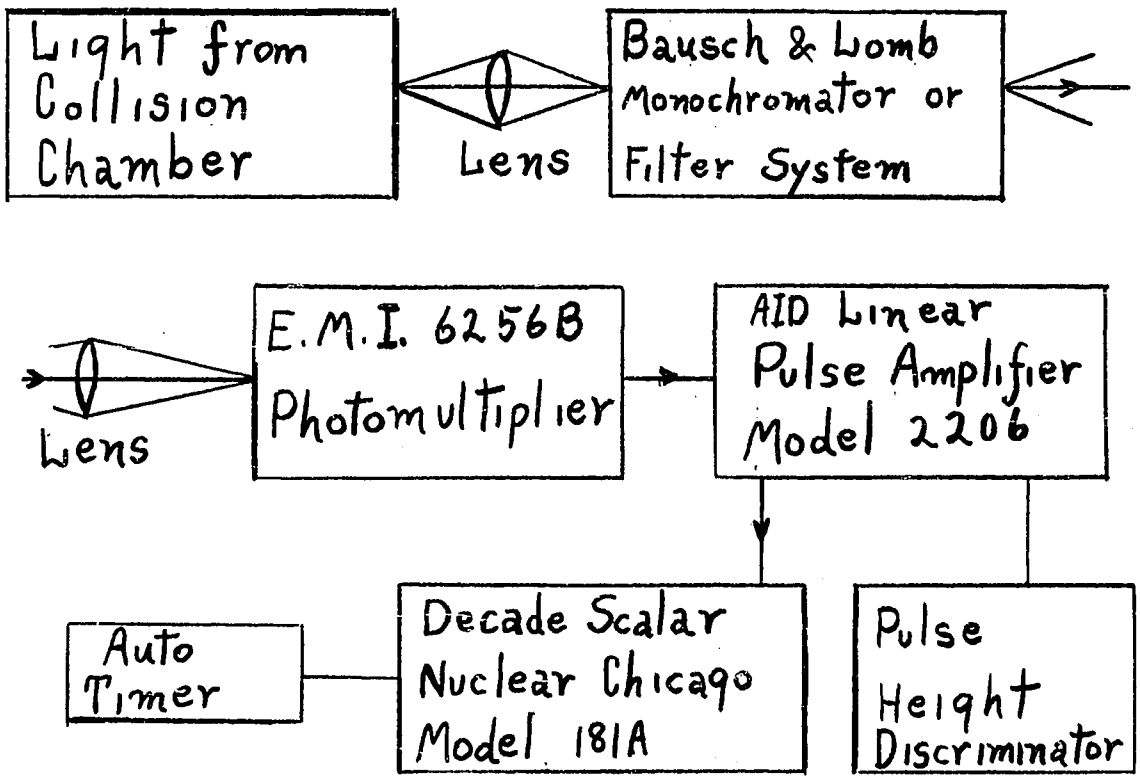

Figure 7. Light Sensing Apparatus

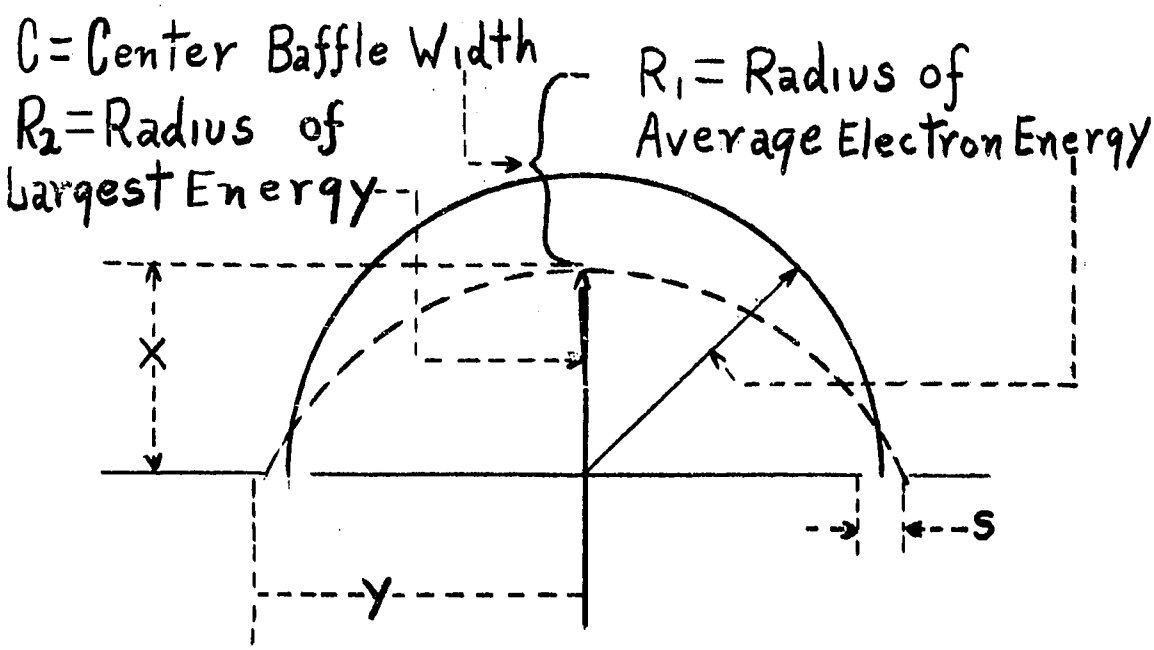

Figure 8. Resolution Diagram for 180° Tube

at an energy E can be determined.

The 180 degree tube had the dimensions, $R_1 = 10$ cm, $C = 1.5$ cm, and $S = .1$ cm.

With these dimensions the energy band transmitted equals 0.1 volts when the electrons have 20 volts of energy.

Energy Resolution of the 90 Degree Tube

The 90 degree tube's resolution was not calculated theoretically but was experimentally measured by a stopping power experiment. The arrangement for the stopping power experiment is shown in Figure 10. This method of measuring the electron energy resolution consisted of making the current collector increasingly negative with respect to the cathode and measuring the current until the collector was sufficiently negative to stop all the current coming from the cathode.

The voltage for which half of the electrons from the cathode were stopped was 1.10 volts for the case when the third anode had a hole of 1.25 mm diameter and the initial electron accelerating voltage was 80. volts. When the hole in the third anode was decreased to .8 mm diameter, half the electrons were stopped with .60 volts.

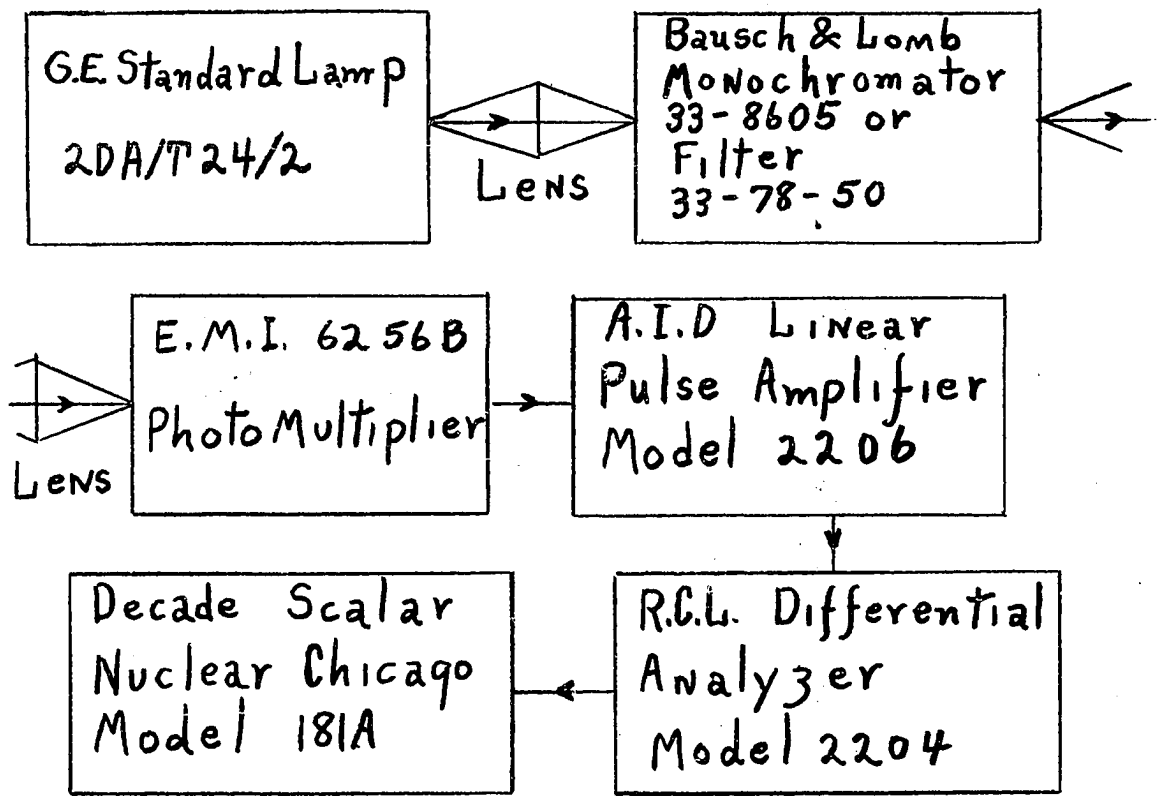

Figure 9. Method of Light Detector Calibration

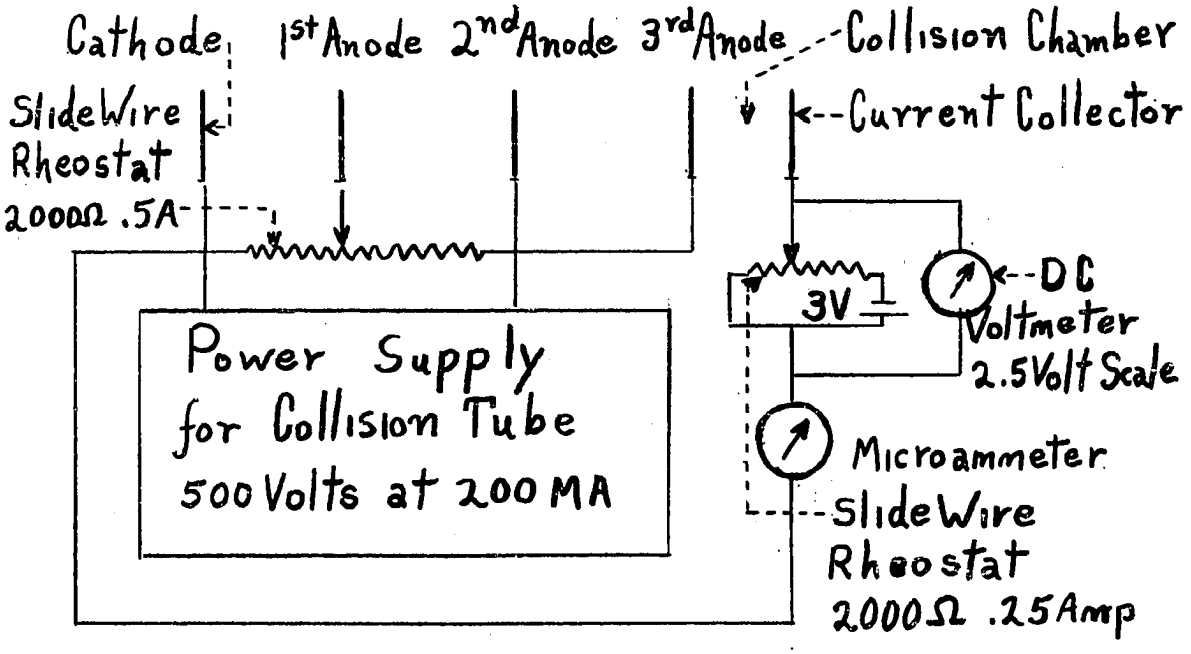

Figure 10. Circuit for Stopping Power Experiment

CHAPTER IV

APPARATUS

The tubes from which the excitation is to be observed are constructed as shown in Figures 11 and 13. The pyrex glass envelope for the 180 degree tube is a semicircle of 10 cm radius with straight extensions on the open ends. The extensions housed the electron-gun assembly and the collector.

To avoid evaporation during bake-out and heat radiated from the cathode, only high temperature resistant materials were used for the metal parts: molydenum, tungsten, tantalum, platinum and ceramics.

The entrance holes at the cathode were .2 mm in diameter. The center baffle was 1.5 cm and the collector opening was .2 mm in diameter.

Between the cathode and center baffle and center baffle and anode a spiral of molydenum wire was inserted and kept at the electrons potential to act as an electrostatic shield. A flat quartz window was sealed to the viewing port at the collision chamber.

The 90 degree tube is similiar in construction to the above 180 degree tube. The difference was that the collector of the 90 degree tube replaced the center baffle of the 180 degree tube. This would be expected to decrease the resolution to some extent and increase the amount of current collected.

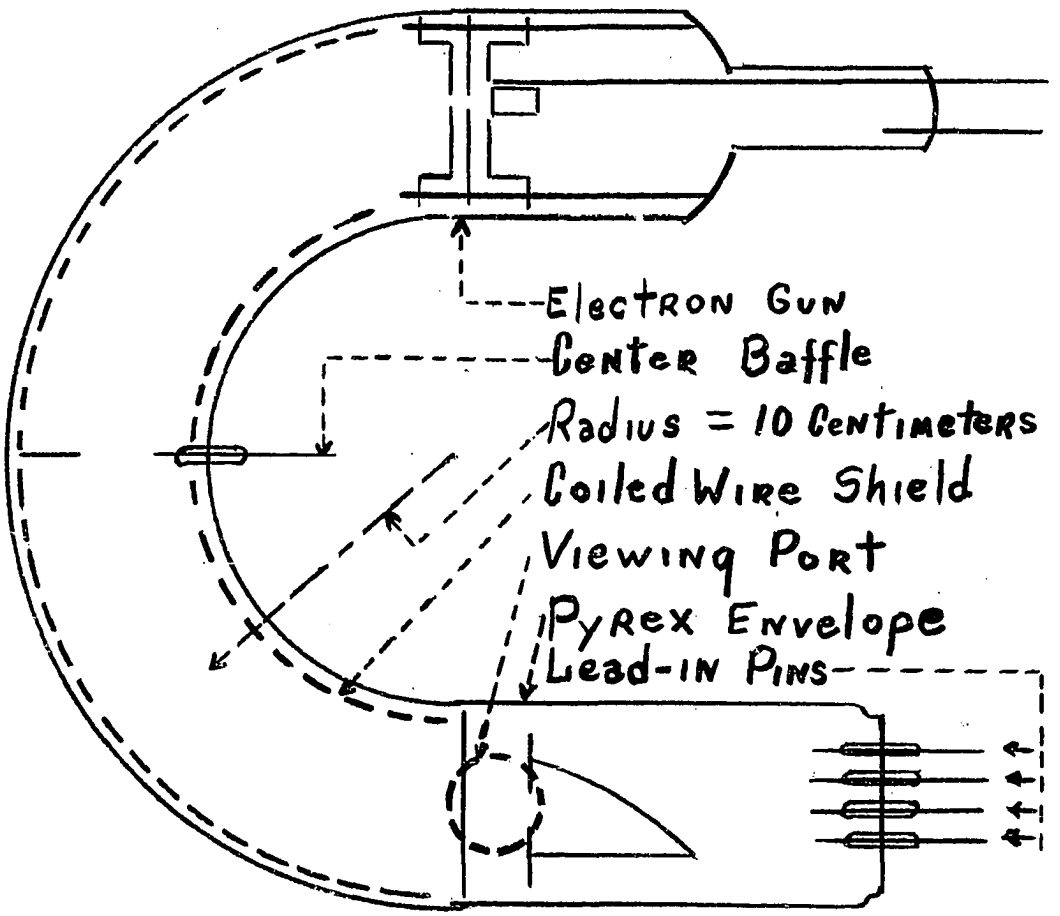

Figure 11. TOP VIEW, 180° Tube

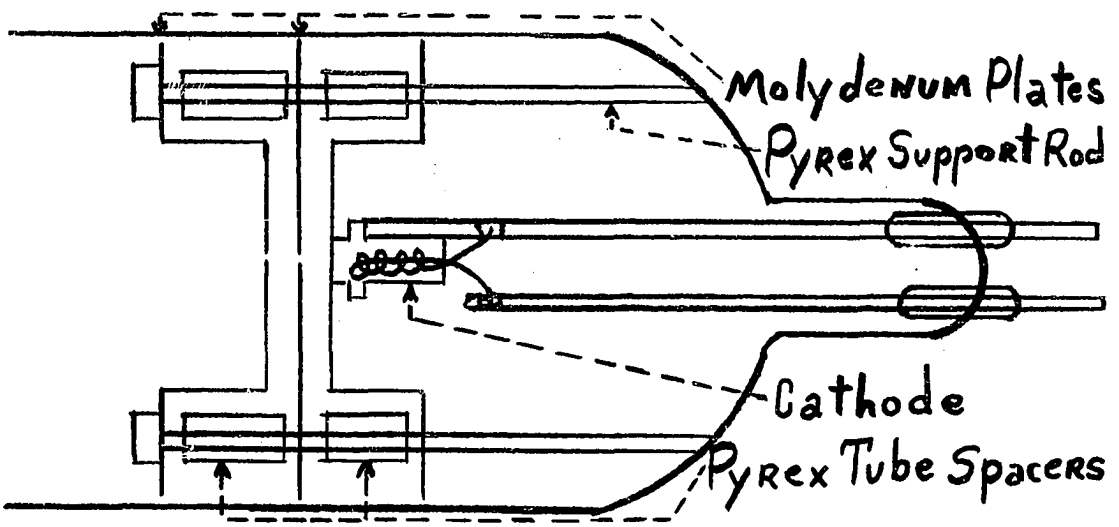

Figure 12. Electron Gun Details

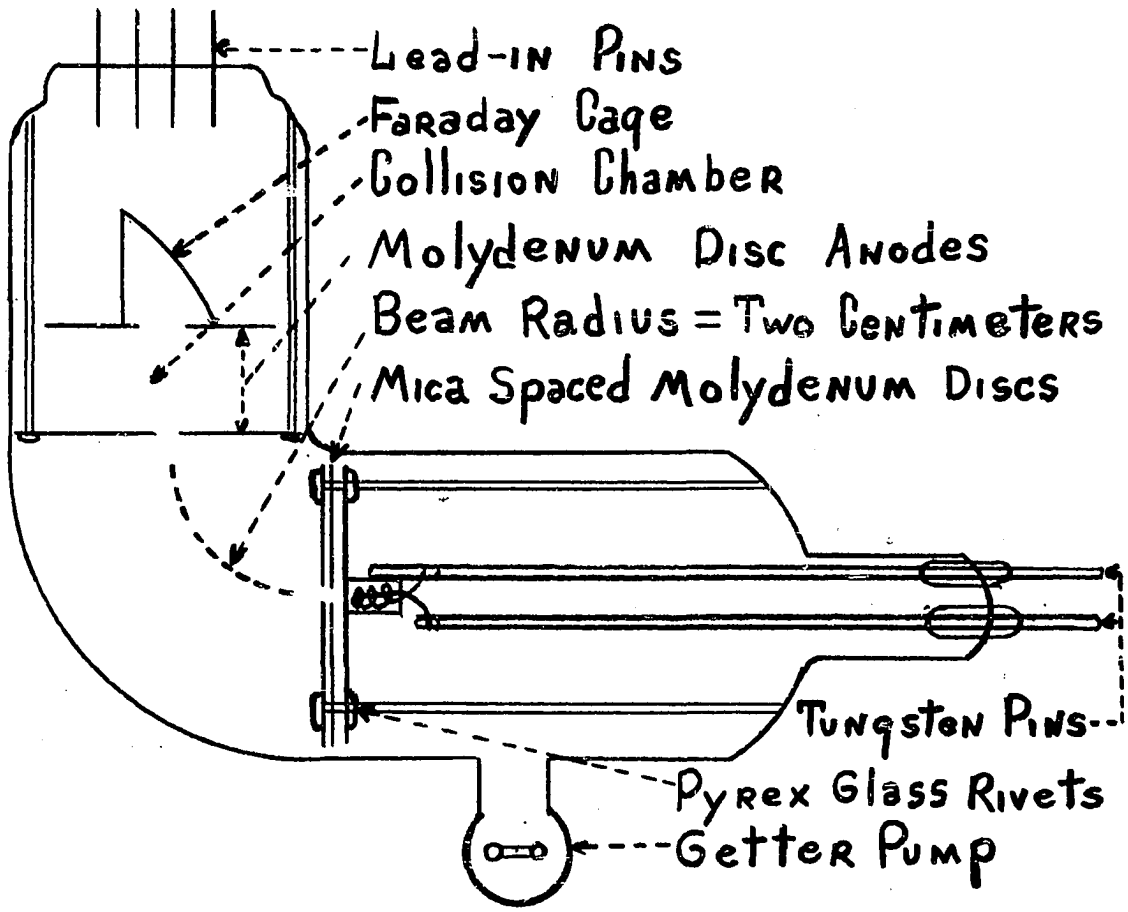

Figure 13. 90° Tube Top View

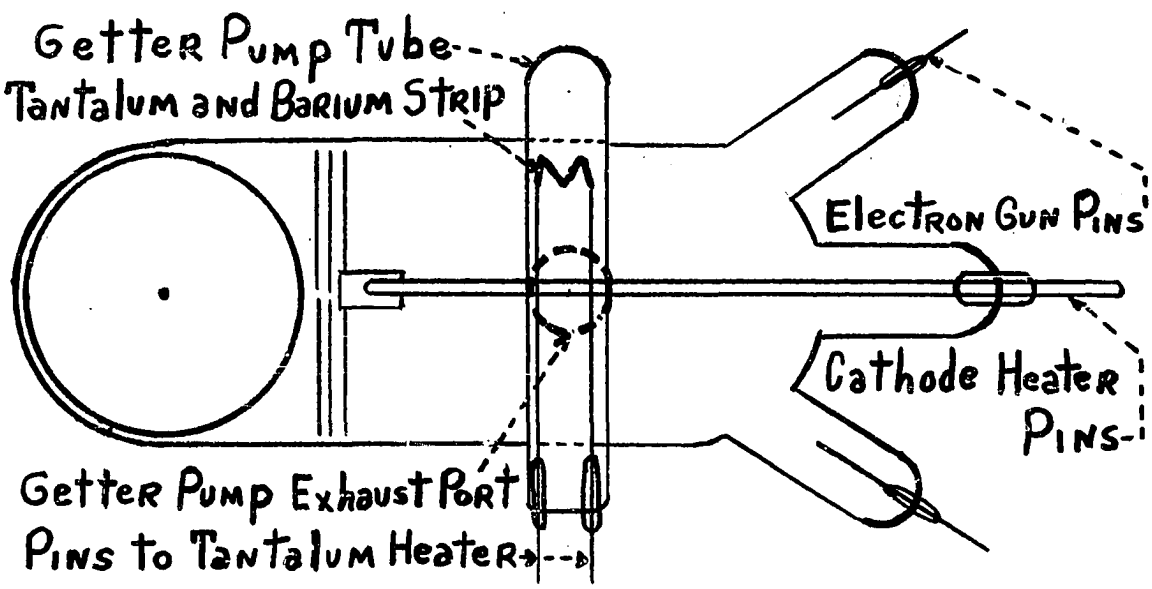

Figure 14. Above Figure rotated 90° into paper

Electron Gun

The electron gun is shown in Figure 12. Two 50 mil. tungsten wires served to support the cathode mechanically and supply the heater current. With this arrangement, one side of the heater was grounded to the cathode. This prevented any tendency for back emission between cathode and heater. This was necessary because barium impregnated cathodes emit from both back and front sides.

The focusing was of the parallel plate electrostatic type. The relation between the convergent electrostatic focal length and the applied voltages and plate separations, to give nearly parallel paths for the electrons emitted from the last accelerating anode is (23),

$$b/a = \frac{(M - 1)\ (M^{\frac{1}{2}} - 1)}{M^{\frac{1}{2}} - \frac{1}{2}}$$

where:

a = distance of cathode from first anode.

b = distance between first and second anodes.

M = ratio of voltage on second to that on first anode.

Coil Details

In order to supply the magnetic field to bend the electron paths for velocity selection, coils were needed which would: allow the field to be varied over a range of from 0 to 15 gauss, provide a uniform field to within a fraction of a per cent over a large area, draw little current and would not warm up or change operating characteristics with time.

A Helmholtz arrangement was used. Two thousand turns of A.W.G. number 22 copper wire was wound on each of two bicycle wheels, 32 cm in

diameter. The tube was then mounted in the center of the Helmholtz coils where the magnetic field was most uniform.

The coils when connected in series had a resistance of 600 ohms. The current supplied was 250. ma for a field of 15 gauss. The coils and tube were oriented with their planes perpendicular to the direction of the earth's magnetic field.

The coils were powered by 6-volt automobile batteries connected in series. A special power supply to be used with the coils is now being constructed. It will be necessary to use this power supply when the colliding electron's energy becomes too large to have the required magnetic supplied by the batteries. The circuit diagram is shown in Figure 15.

Details of the Ultra-High Vacuum System

In order to attain as high a vacuum as possible, to keep the impurity level low when the helium gas is introduced, a Westinghouse type ultra-high vacuum system (1) was constructed. Pressures as low as 5 X 10^{-11}mm of mercury were attained with it. A general description was given in the preceding chapter.

The three stage oil diffusion pump was built in the glass-shop. Its stage openings were a little larger than usual because it was designed to be backed by a megavac fore pump, allowing a little lower ultimate pressure to be achieved by the system. The general lay-out of the vacuum system is given in Figure 17.

A special oven was constructed to bake the vacuum system. It has a self-regulated heating element. After each bake-out, the ion gauge was out-gassed for about 30 minutes by resistance heating.

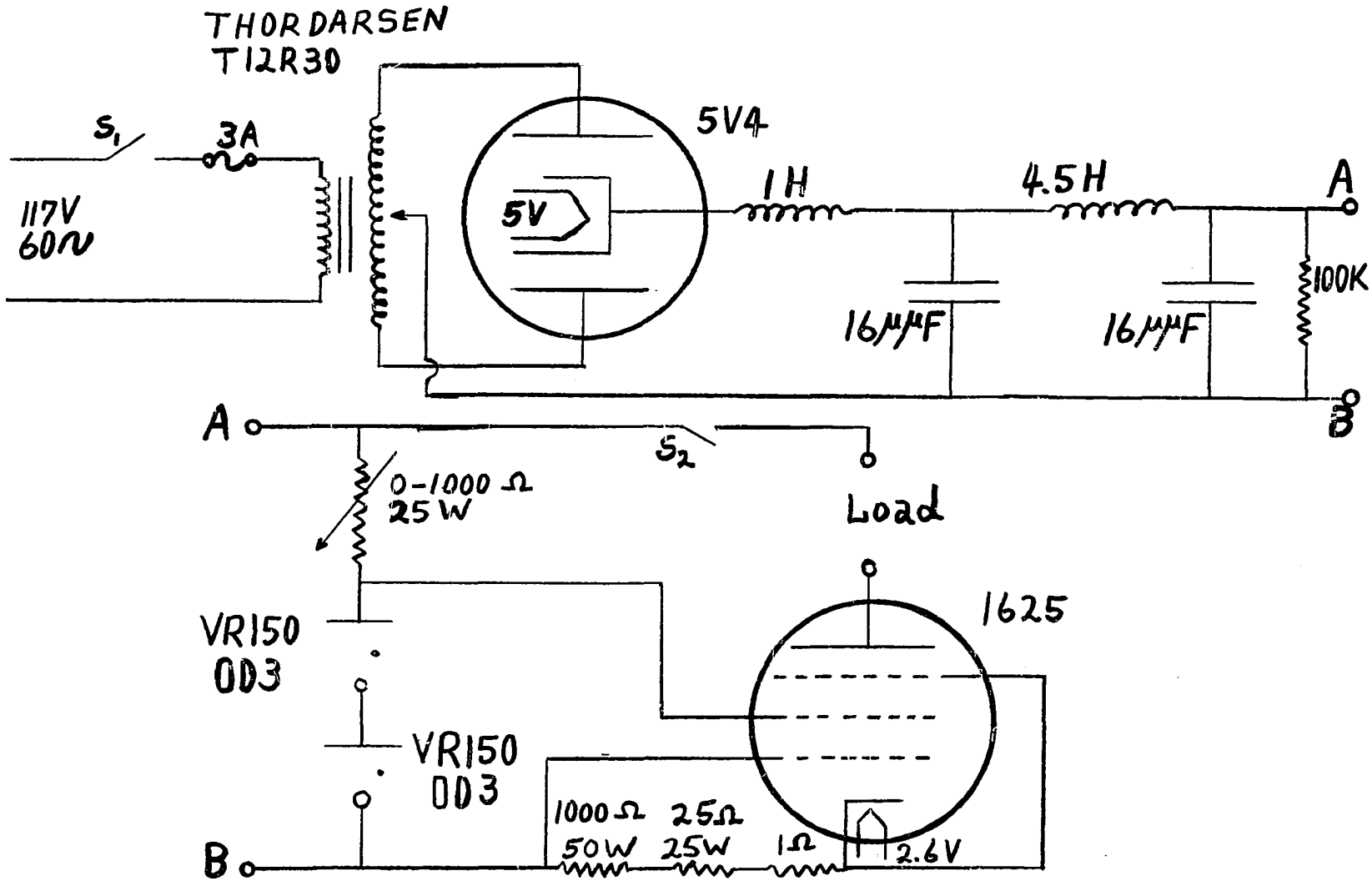

Figure 15. Power Supply for Coils

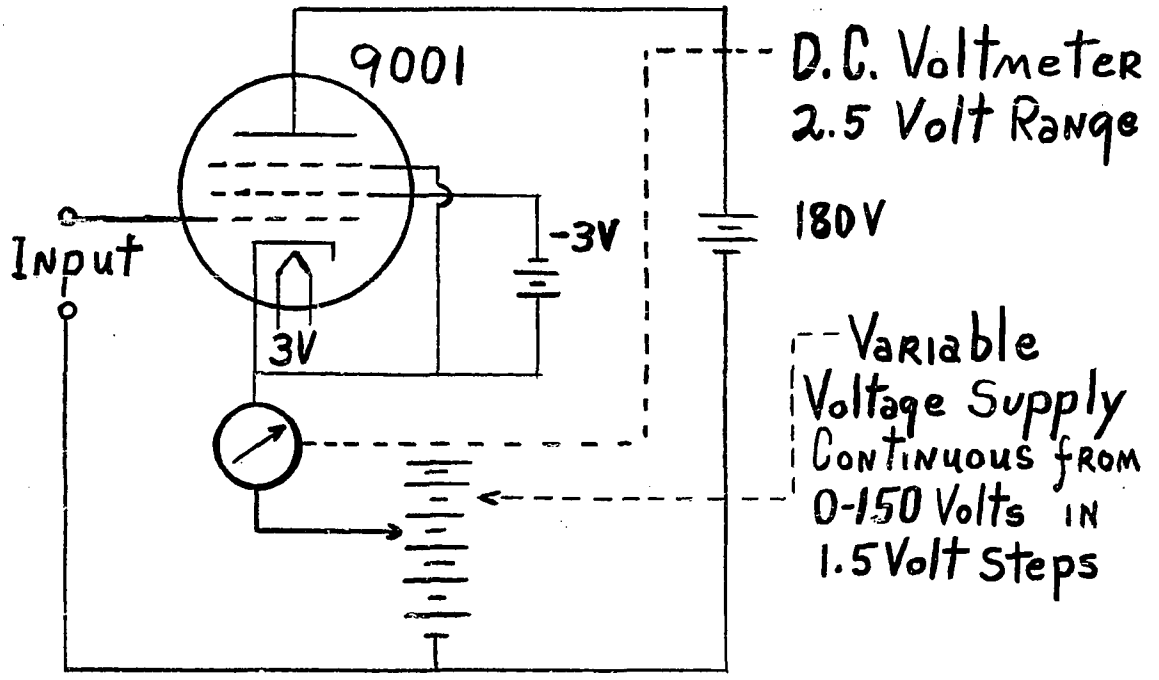

Figure 16. Extended Range Voltmeter

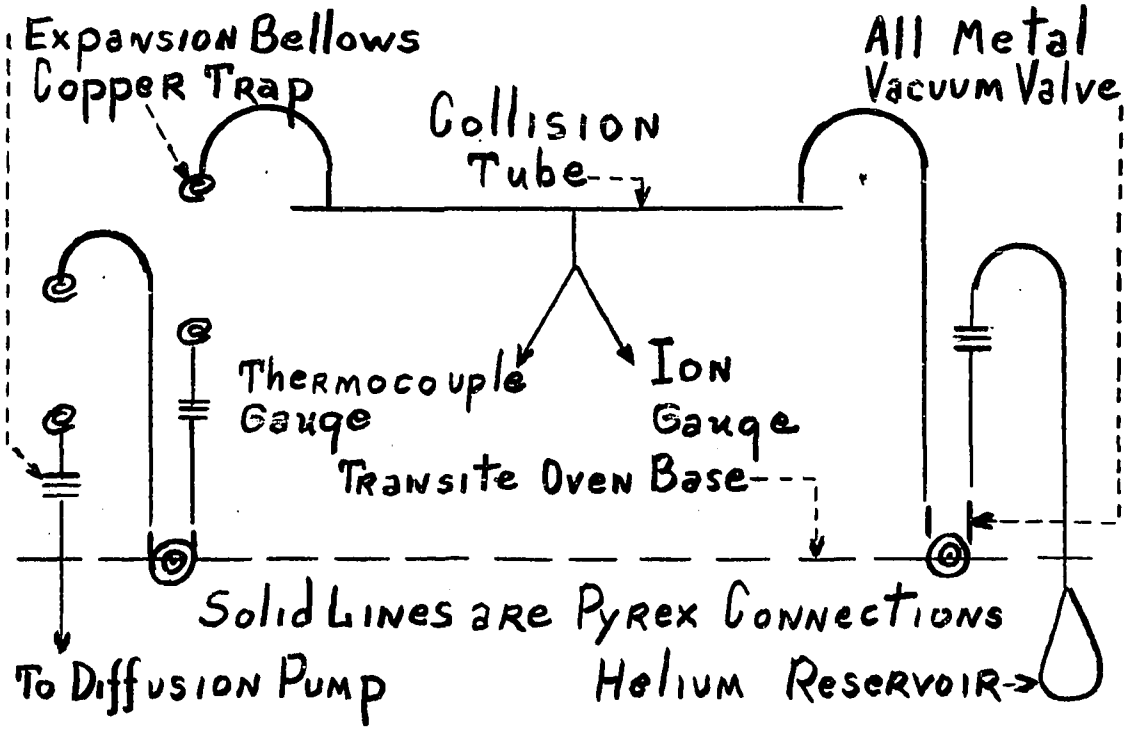

Figure 17. Ultra High Vacuum System

Power Supply for Ion Gauge

A power supply with an out-gas switch was built for the ion gauge and is shown in Figure 18.

Electrometer

Since the currents to be measured by the ion gauge at pressures of 10^{-11}mm of mercury are around 10^{-10} amperes and since it is desired that the measuring instrument hold its calibration curve for months, a special electrometer was designed. It consisted of three stages of cathode follower operation.

The circuit together with its power supply is shown in Figure 19. The circuit uses RCA 954 type tubes operated at below normal conditions. At these operating conditions the RCA 954 has an input resistance of about 10^{14} ohms. This means the electrometer can be used to measure currents as small as 10^{-14} amperes.

Power Supply for the Excitation Tubes

The power supply for the main collision tubes had to be one which would regulate to within .1 volts at a voltage range from 200 to 500 volts and a current drain of from 100 to 300 milliamperes. The circuit diagram is given in Figure 20.

Photomultiplier Circuit

The photomultiplier interstage resistors and capacitors were mounted in vacuum and chilled to liquid air temperatures together with the photomultiplier. Ten DeKhotinsky cement seals were used in bringing the various leads out of the refrigerator to the batteries. The circuit diagram together with the various interstage voltages are given in Fig-

ure 21.

Extended Range Vacuum Tube Voltmeter

A continuous monitor voltmeter was needed to measure the accelerating voltages over the range from 10 to 200 volts with .01 volt accuracy. The instrument was built according to the circuit diagram given in Figure 16.

Pyrex Demountable Photo-Multiplier Refrigerator

The measurement of extremely low levels light flux requires refrigeration of the photomultiplier to liquid air temperature to reduce the thermionic and caesium vapor pressure dark current components. It is convenient to have the photo-multiplier tube in a vacuum and the refrigerator demountable so that the photo-multiplier can easily be withdrawn and minor adjustments made. Ease of construction and adaptability to the many different types and sizes of photo-multiplier tubes is also desired.

The refrigerator described here is an all glass type designed especially for an EMI type tube. The EMI 6256B has the photo-sensitive cathode in the end and has approximate dimensions of 5 (length) inches by 2 (diameter) inches. The same refrigerator can be adapted to the RCA 1P21 tube by a minor change to be explained after describing the refrigerator.

Referring to Figure 22, the only section which is not evacuated under operating conditions is the part of the inner sphere which does not include the photo-multiplier housing.

This section is the liquid air reservoir. It has a capacity of

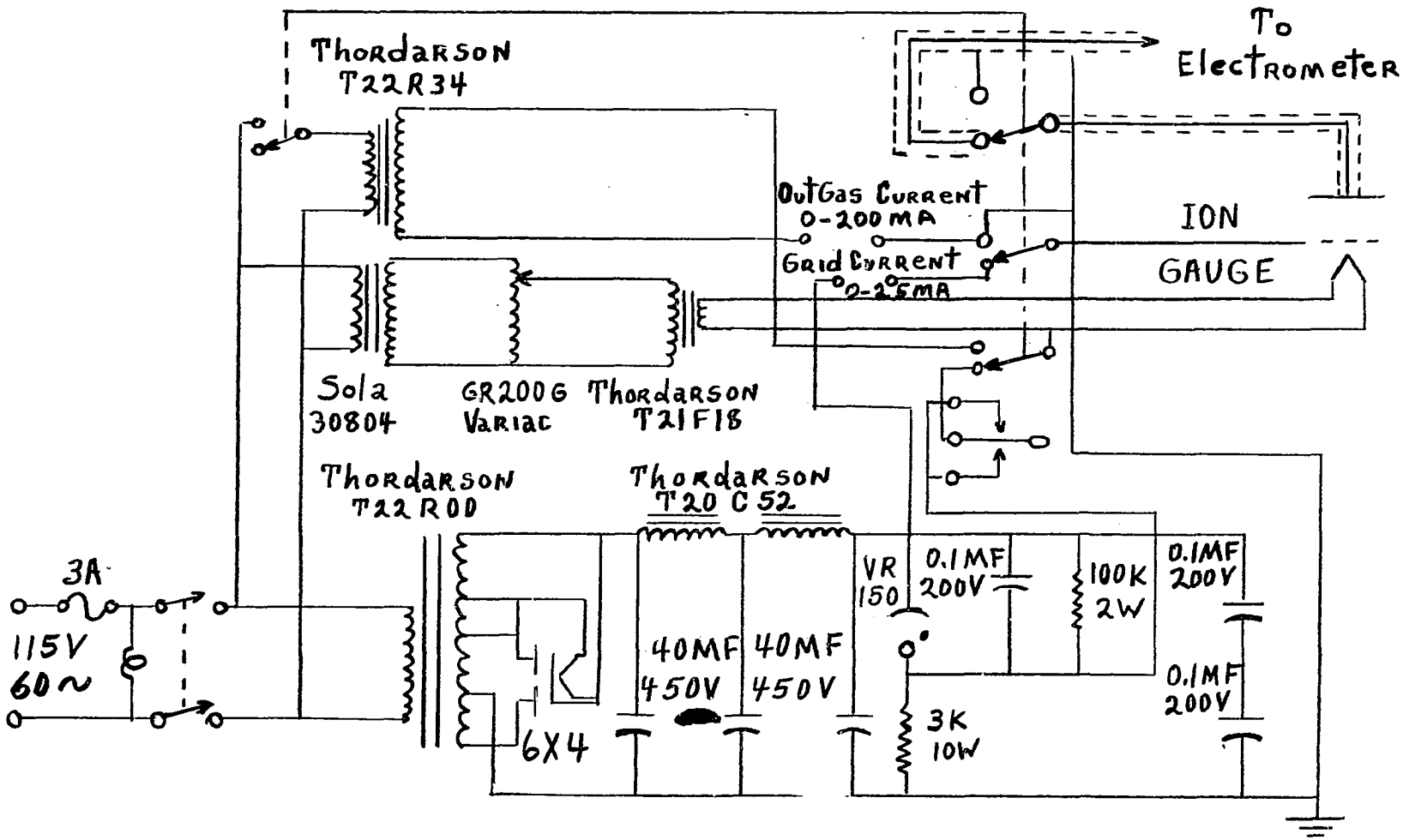

Figure 18. Power Supply for Ion Gauge

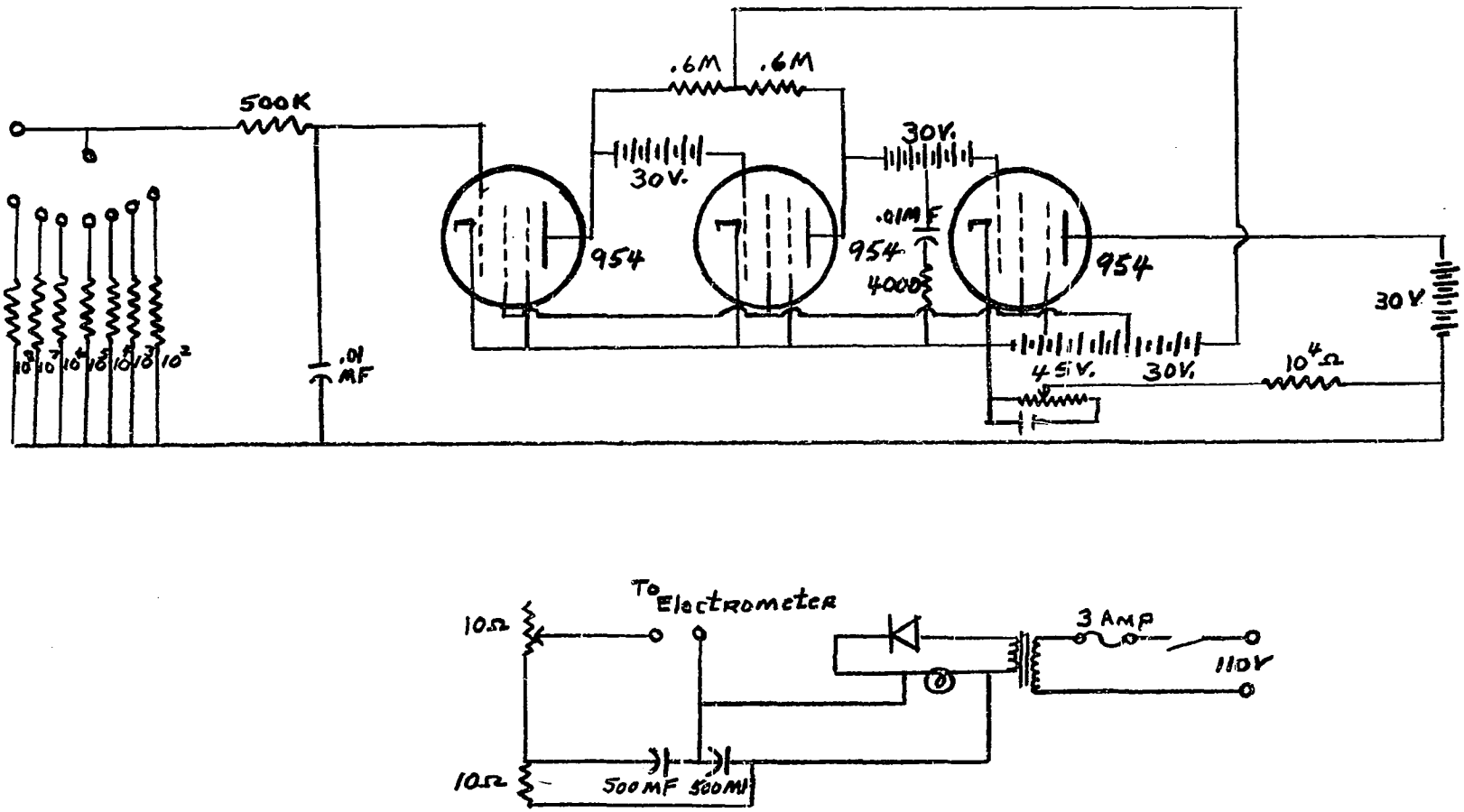

Figure 19. Electrometer and Electrometer Power Supply

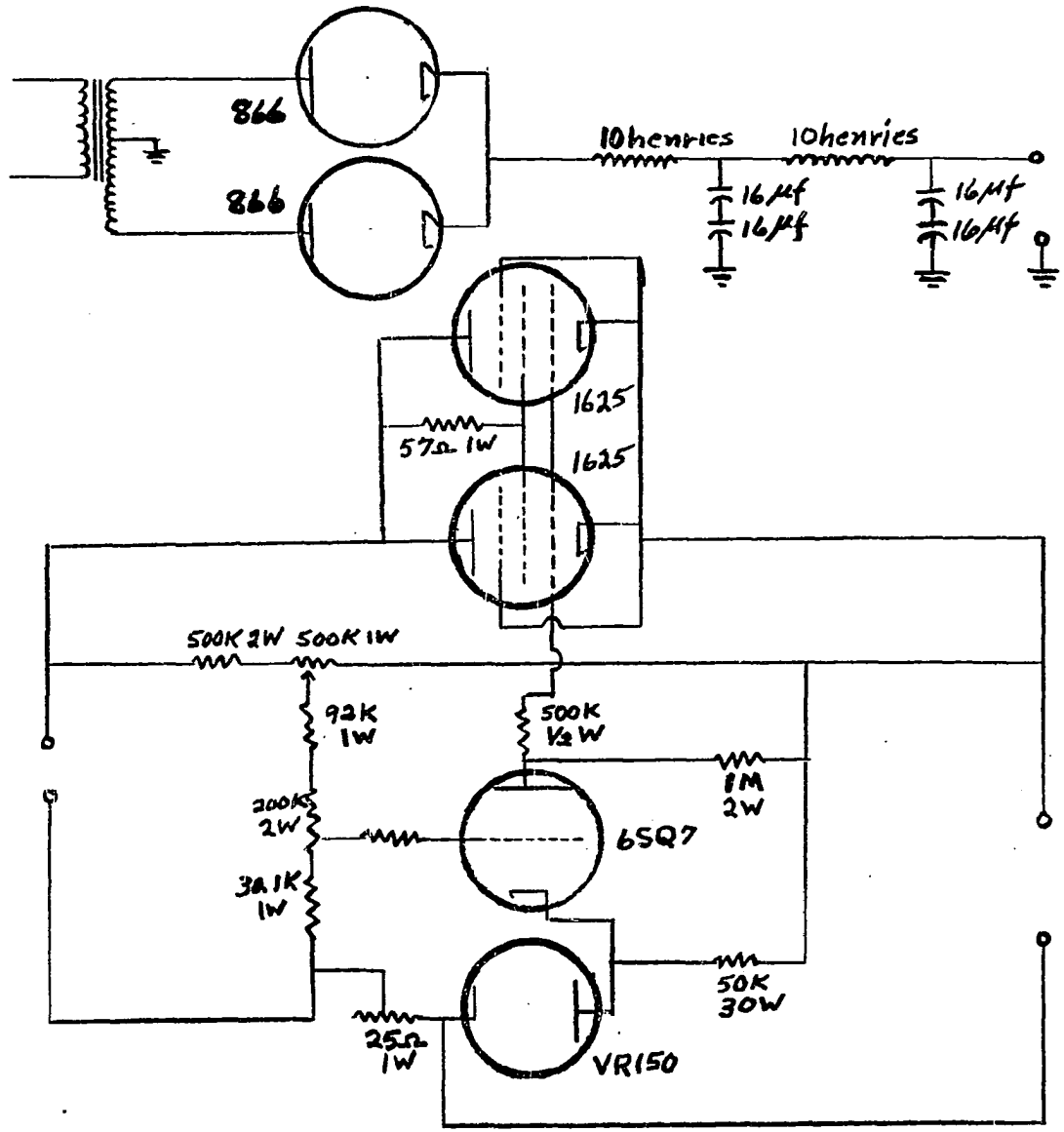

Figure 20. Power Supply for Collision Chamber

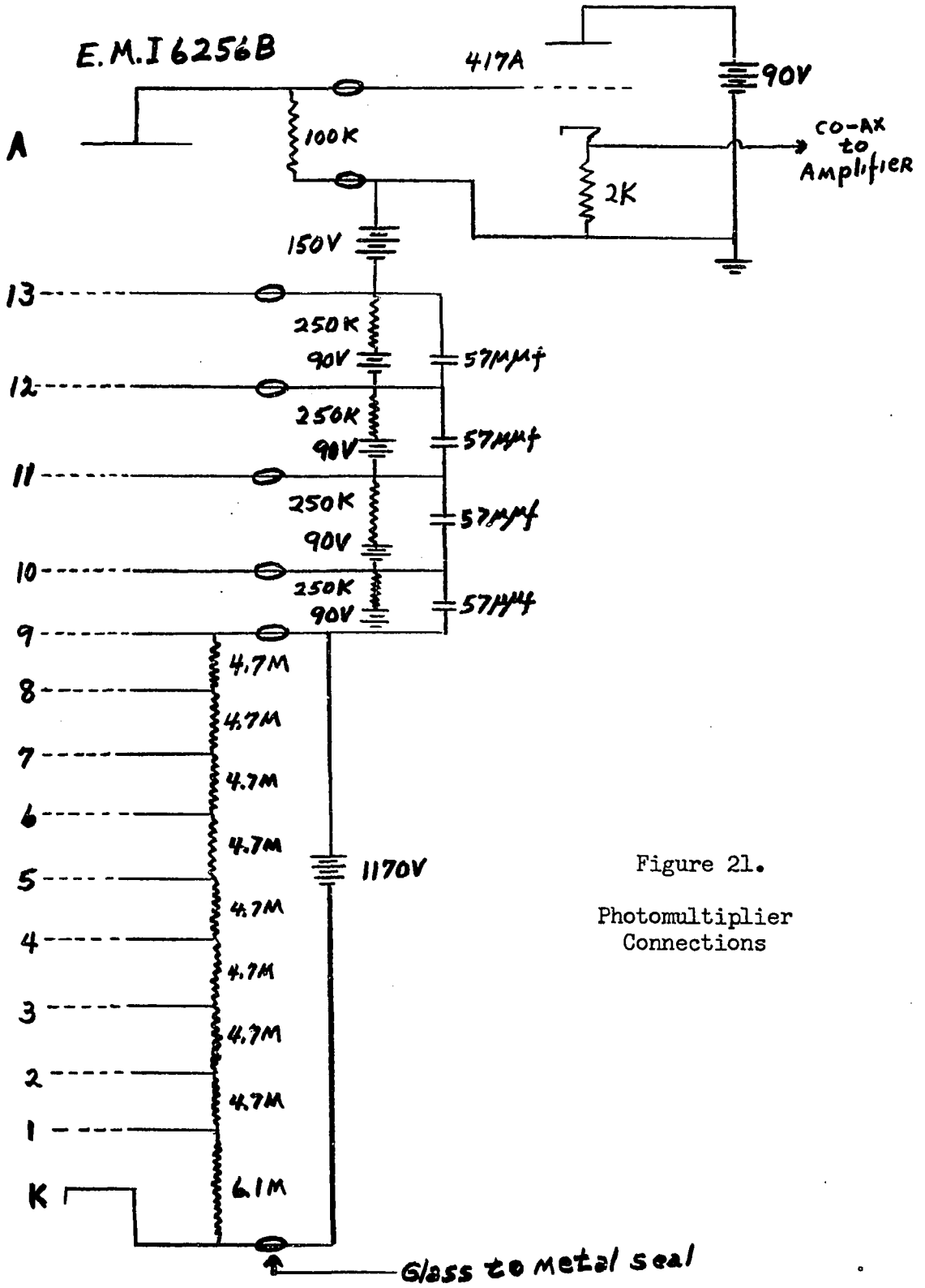

Figure 21.

Photomultiplier
Connections

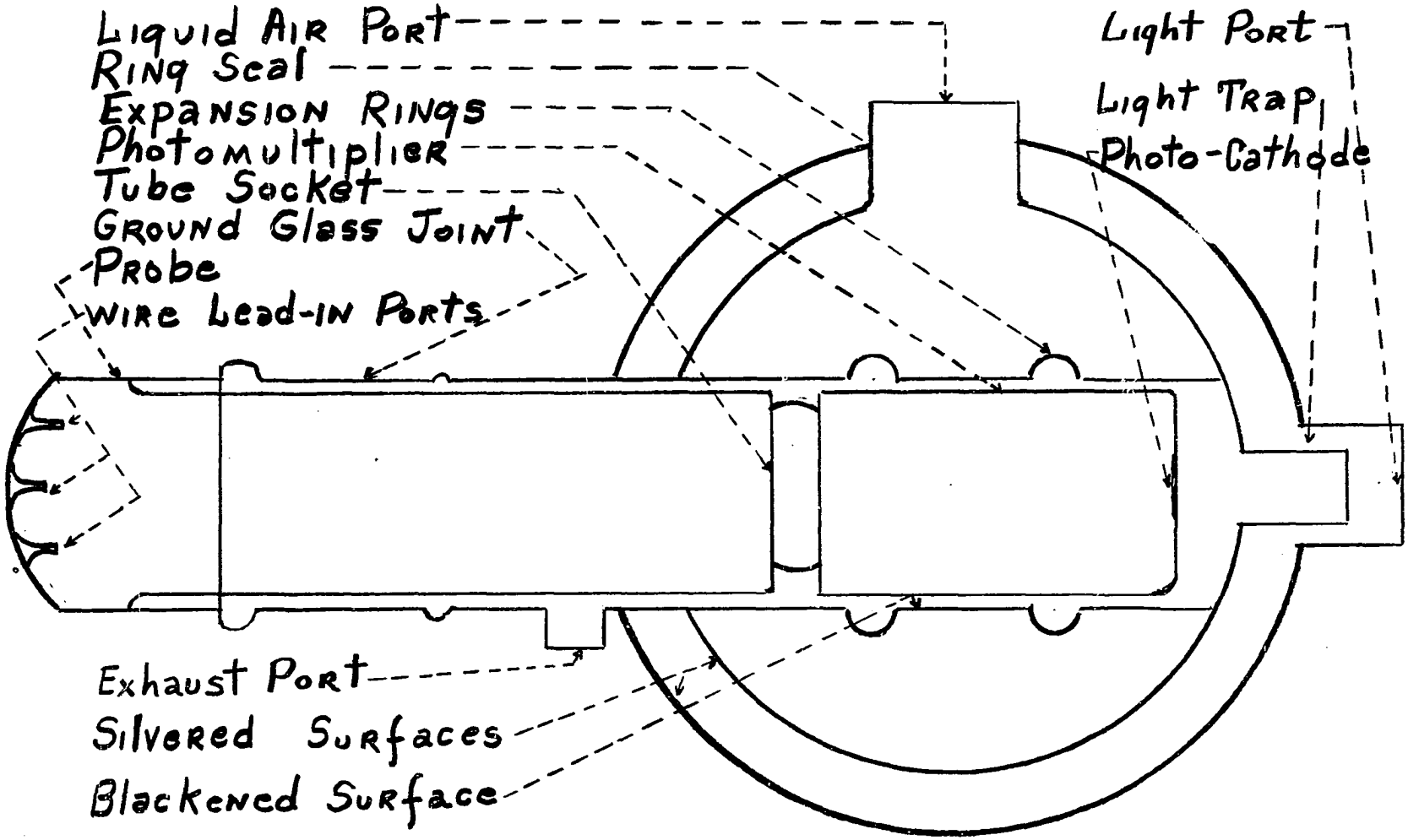

Figure 22. Photomultiplier Refrigerator

approximately one and one half liters. The ground glass joint was a 60/50 standard taper type. The photomultiplier was mounted on the male ending of this joint in the manner of a probe. Stop cock grease made the joint vacuum tight. One is not bothered by stop cock grease vapor condensing on the photo-tube because of the liquid air temperature. The light port can be made of a quartz to pyrex graded seal if it is necessary to view ultra-violet light.

The refrigerator can be adapted to the RCA 1P21 by sealing the light port and light trap tube to the spheres at right angles with respect to the probe.

The materials required for making the refrigerator are: one standard taper 60/50 pyrex ground glass joint, a 3000 milliliter pyrex flask and a 2000 milliliter pyrex flask together with various sizes of pyrex tubing.

Because of the low thermal conductivity of glass, efficient use is made of the liquid air in maintaining the photo-multiplier at liquid air temperature. One liter of liquid air was required to cool the refrigerator from room temperature to that of liquid air and an additional liter was added approximately every five hours to maintain liquid air temperature. No difficulty was experienced obtaining and holding a hard vacuum of 10^{-6} millimeters of mercury pressure. Using this refrigerator and the EMI 6256B type tube, the dark counts were reduced to less than one half count per second with no pulse height selection.

CHAPTER V

CALIBRATION OF EQUIPMENT

Calibration of Pressure Measuring Devices

The ion gauge and thermocouple gauge were calibrated using a McCleod gauge. The calibration data for the thermocouple gauge is given in Table I. The ion gauge was calibrated using a McCleod gauge until the ion gauge's calibration curve became linear with pressure. After the ion gauge reached its linear region, an extrapolation was used to complete the curve at pressures too low for the McCleod gauge to measure. The ion gauge calibration data is given in Table II.

Efficiency of Light Intensity Measuring Apparatus

To measure the number of photons coming out of the excitation tube per second in the manner described in Chapter II, requires knowing the solid angle subtended by the first lens, the light transmitting efficiency of the monochromator or filter system as a function of wave length being the counting efficiency of the photomultiplier tube, and the number of pulses biased out by the pulse height selector.

The method used to find the product of the monochromator or filter system transmission, the photomultiplier tube efficiency, and the fraction of pulses passed by the linear amplifier for various wave lengths is indicated in the block diagram of Figure 7.

TABLE I

VOLTAGE AND PRESSURE RELATIONSHIP FOR THERMOCOUPLE GAUGE

Voltage (volts x 10^{-5})		Pressure (mm Hg)
132		3×10^{-1}
267		1.7×10^{-1}
417		6.5×10^{-2}
523		5.3×10^{-2}
507		4.9×10^{-2}
604		3.1×10^{-2}
655		2.5×10^{-2}
660		2.3×10^{-2}
693		2.1×10^{-2}
727	Tube: RCA 1946	1.5×10^{-2}
768	Current: 50 ma	1.1×10^{-2}
778	Gas: Helium	9.2×10^{-3}
785		8.2×10^{-3}
805		6.3×10^{-3}
811		$6. \times 10^{-3}$
825		5.5×10^{-3}
841		3.2×10^{-3}
838		3.1×10^{-3}
852		2.4×10^{-3}
865		2.0×10^{-3}
862		1.8×10^{-3}
875		1.2×10^{-3}

TABLE I--Continued

Voltage (volts x 10^{-5})	Pressure (mm Hg)
872	1.0×10^{-3}
883	3.5×10^{-4}
888	$4. \times 10^{-5}$
894	$8. \times 10^{-6}$

TABLE II

CURRENT AND PRESSURE RELATIONSHIP FOR IONIZATION GUAGE

Current (Amps x 10^{-6})		Pressure (mm Hg)
47		3.2×10^{-3}
30		1.6×10^{-3}
25		1.4×10^{-3}
23		8×10^{-4}
19		5.8×10^{-4}
18		$4. \times 10^{-4}$
15		2.5×10^{-4}
14		$2. \times 10^{-4}$
11		1.5×10^{-4}
5.1	Tube: Westinghouse WL-5966	9.5×10^{-5}
4.4	Grid Current: 10 ma	9.2×10^{-5}
4.0	Gas: Helium	3×10^{-5}
3.2		2.5×10^{-5}
3.1		2.3×10^{-5}
2.5		1.9×10^{-5}
1.2		$1. \times 10^{-5}$
.12		$1. \times 10^{-6}$
.012		$1. \times 10^{-7}$
.0012		$1. \times 10^{-8}$
.00012		$1. \times 10^{-9}$
.000012		$1. \times 10^{-10}$
.0000012		$1. \times 10^{-11}$

A ribbon filament type 20A/T24/2 pyrometer standard lamp was purchased from General Electric Company which had its tungsten filament temperature calibrated in terms of the filament current. This was done with an optical pyrometer at the company.

From Planck's equation one can calculate the number of photons emitted in a narrow spectral range for a given temperature of the filament per unit area. Knowing the temperature and filament area of the standard lamp, one can now calculate the number of photons incident on the monochromator entrance slit.

Overall Counting Efficiency Using the Monochromator

The energy band pass for the monochromator for various slit openings was supplied by the Bausch and Lomb Company. It was necessary to know this band pass because the overall efficiency for one wavelength was needed.

The overall efficiency ratio of the photon counting system is the ratio of the number of photons counted to the number incident on the monochromator entrance slit for a particular wave length.

Table III gives the variation of the overall efficiency ratio with wave length while using the monochromator with a linear amplifier bias of 2.50.

Overall Counting Efficiency Using the Filter System

When the Bausch and Lomb 33-86-05 monochromator is replaced by the filter system in the above calibration, the overall efficiency, for the wave length 5000 angstroms and a .50 bias on the linear amplifier, was found to be 3.60×10^{-3}. The filter system consisted of a Bausch

and Lomb 33-78-50 interference filter together with a Wratten number 4 in B glass, and a Wratten 45 in B glass. Their combined transmission properties are given in Table IV.

Optimizing Pulse Height Selection with a Differential Analyzer

Engstrom (5) has shown using a differential analyzer that noise pulse heights are on the average smaller than photon produced pulse heights. This makes it advantageous to use pulse height discrimination. This also biases out part of the signal but it has been accounted in the overall counting efficiency ratio discussed above.

With the differential analyzer one can count the pulses arising from signal in a given spectral range plus background pulses or only background pulses with and without bias to determine the ratio of signal to noise with and without bias. By measuring the energy distribution of the signal pulses and the energy distribution of the dark pulses, the point of optimum bias can be deduced. This is the point which will give the largest signal to noise ratio.

TABLE III

TABLE OF OVERALL EFFICIENCY

Wavelength (Angstroms)		Overall Efficiency Ratio
3600		1.4×10^{-3}
3800		5.4×10^{-4}
4000		2.0×10^{-4}
4200		1.0×10^{-4}
4400		6.2×10^{-5}
4600		4.6×10^{-5}
4800		3.2×10^{-5}
5000		2.3×10^{-5}
5200	Bausch and Lomb	1.9×10^{-5}
5400	33-86-05 Quartz	1.86×10^{-5}
5600	Monochromator	1.9×10^{-5}
5800		1.6×10^{-6}
6000		1.27×10^{-6}
6500		6.2×10^{-7}
7000		2.38×10^{-7}
8000		6.3×10^{-8}

TABLE IV

TRANSMISSION PROPERITIES OF THE COMBINED FILTERS

Wavelength (in Angstroms)	Per cent transmission of No. 4 Wratten and interference filter
4500	0
4600	.0004
4700	.010
4800	.019
4900	.0584
4950	.124
5000	.277
5016	.292
5050	.215
5100	.077
5200	.0218
5300	.010
5400	.0075
5500	0

CHAPTER VI

OPERATIONAL PROCEDURE

After the system had been baked out at 400° for a period of four hours, the copper traps were clean. Any residual absorbable gas was continuously absorbed. After the ion gauge had been out-gassed for 30 minutes, the valves were closed and the ion gauge was left pumping for about two hours. The pressure was then about 10^{-10}mm of Hg. Helium was let in the system to a pressure of about 10^{-3}mm Hg and again the system was pumped out further reducing any residual foreign gas.

The major portion of the contamination to the system after the above process came from the hot cathode. Since during bake-out the metal parts of the system were baked out to only 400°, the cathode and adjacent anodes evolved a considerable amount of gas for a period of several hours after the cathode was elevated to its operating temperature of around 1000° C.

The temperature of the cathode was initially raised slowly so that the gas pressure did not get high enough to saturate the copper traps before it was pumped out. The cathode was then raised to a temperature slightly above the normal operating temperature, so that the rate of evolvement was small when the temperature was finally lowered to operating conditions. It was usually easier to out-gas a Phillips type cathode than an oxide cathode.

Optical Alignment

The system was aligned along the geometric centers of the optical apparatus for data taking. The optical apparatus was also calibrated along geometric rather than optical centers.

Dark Counts

The room was kept dark except for the light coming from the cathode and the more distant electronic gear. A measure of the dark current was taken with conditions identical to those when a signal count was taken except the anode voltage was removed. At intervals of about three signal measurements, the dark current was again measured to check for dark current drift.

Statistics

Since the chance that an electron will excite an atom and thereafter the atom radiate a photon is a random event, the reliability of the count was given by the standard deviation. This means the expected statistical error decreased with increasing count time for any one count rate. However as the count time was increased the chances for variation of the experimental parameters such as tube current, pressure, etc., increased. The optimum count time for this experiment was judged to be five minutes.

The pressure was checked before and after each measurement. A continuous monitor was kept on tube current and voltage. Any variations of the magnetic field also showed up as variations in the tube current. After each measurement the helium was pumped out and a fresh helium dose was added.

All pertinent data were recorded after each measurement.

CHAPTER VII

RESULTS OF OBSERVATIONS ON HELIUM

Experimental Conditions

In order to obtain results which were not influenced by secondary effects (such as resonance radiation, exciting more than one atom with an electron, etc.), graphs were made of the counting rate as functions of the pressure and current for the line 5016A of helium. The data was taken for both the 180 and 90 degree tubes.

Line Intensity vs. Beam Current

In order to determine that the electrons make only one collision while passing through the collision chamber, the graphs of the intensity versus electron current were made. A graph will be linear if each electron makes no more than one collision. This linearity is important because after an electron has made a collision its energy is changed.

Line Intensity vs. Pressure

In order to avoid the secondary effects due to pressure discussed in Chapter II, the pressure graphs for helium line 5016A were made. The results for the 180 and 90 degree tubes are discussed separately below.

Results for the 180 Degree Tube

The results taken for the 180 degree tube were taken using the monochromator instead of the filter system used with the 90 degree tube.

The signal from 180 degree was much weaker than the 90 degree tube due to the smaller solid angle sustended by the slit of the monochromator. The line factor for these curves is 1.09 X 10^{-20} cm^2/ count / microampere. This means the count rate multiplied by the factor for 15 microamperes of current gives the excitation cross-section in units of square centimeters.

Figure 23 shows the counting rate versus current curve to be linear; thus double excitation does not occur.

Figure 25 shows the counting rate versus incident electron current. The pressure does not intersect the axis as reported by Lees but is still measurable at pressures lower than 10^{-4}mm Hg. The curve appears to become straight below 5 X 10^{-3}mm Hg.

The excitation function shown in Figure 24 taken with the 180 degree tube is doubtful due to variations in pressure while taking the data. This function for the 90 degree tube is treated in Chapter VIII.

Results for the 90 Degree Tube

Figure 26 shows the electron beam current as a function of the counts per second for the 90 degree tube. As is shown above the number of counts per second is proportional to line intensity.

Table V shows the variation that is tabulated from another day's run. The third column shows all data reduced to a common pressure.

Figure 27 shows the pressure versus count rate dependency measured experimentally. The middle region and the low pressure linear region are shown. It is seen that the curve approaches linearity for pressures of 5 X 10^{-3}mm Hg or less.

Table VI shows data tabulated for showing the pressure dependency.

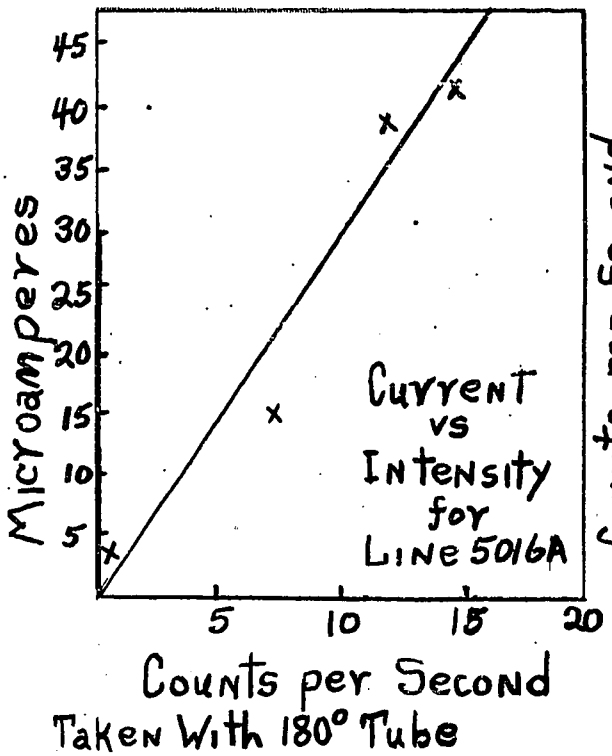

Figure 23

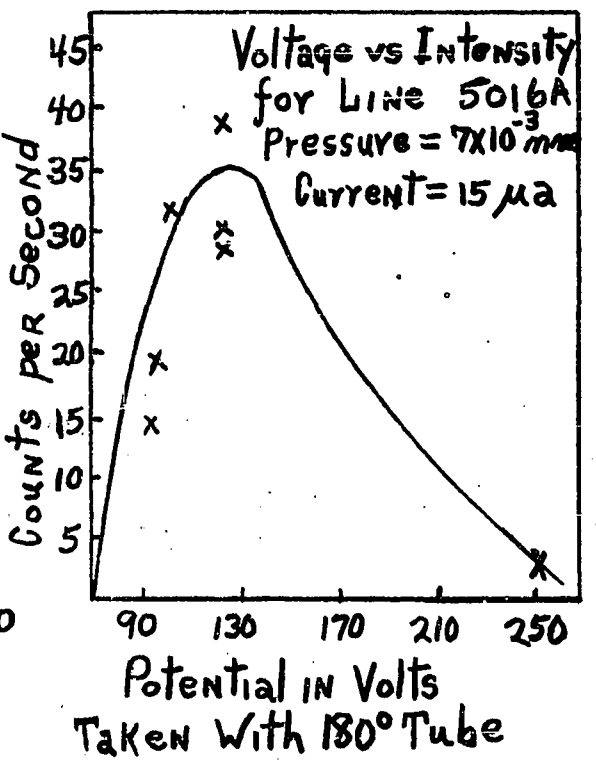

Figure 24

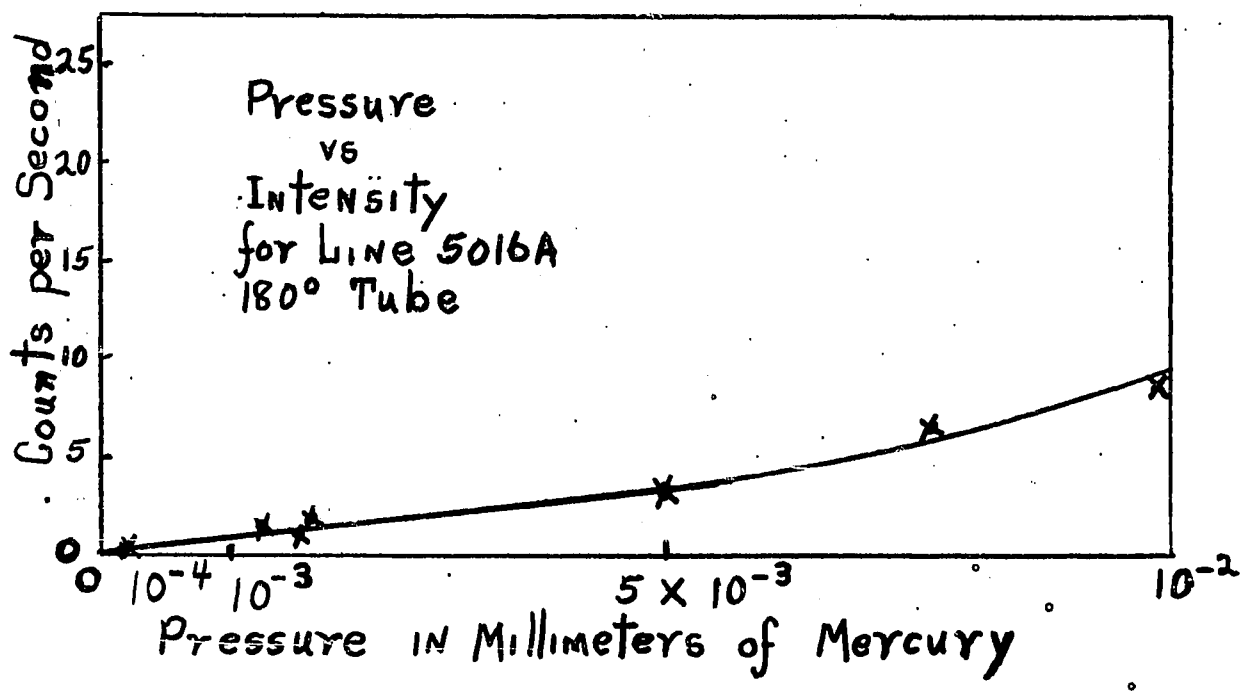

Figure 25

TABLE V

VARIATION OF COUNT RATE WITH CURRENT FOR HE LINE 5016

Taken with: Voltage = 150 volts
Pressure = 50 X 10^{-3}mm Hg
90 Degree Tube

Current (microamperes)	Counts/Sec/5 X 10^{-3}mm Hg
1.1	1730
1.30	945
2.80	1880
3.0	2160
3.1	2290
3.95	3410
5.95	3290
6.50	3580
7.6	5060
7.65	5050
7.85	4340
9.35	4620
9.6	4730
11.5	5650
11.6	5470
13.9	7000
15.25	7380
15.35	7620
17.25	8900
18.85	9850

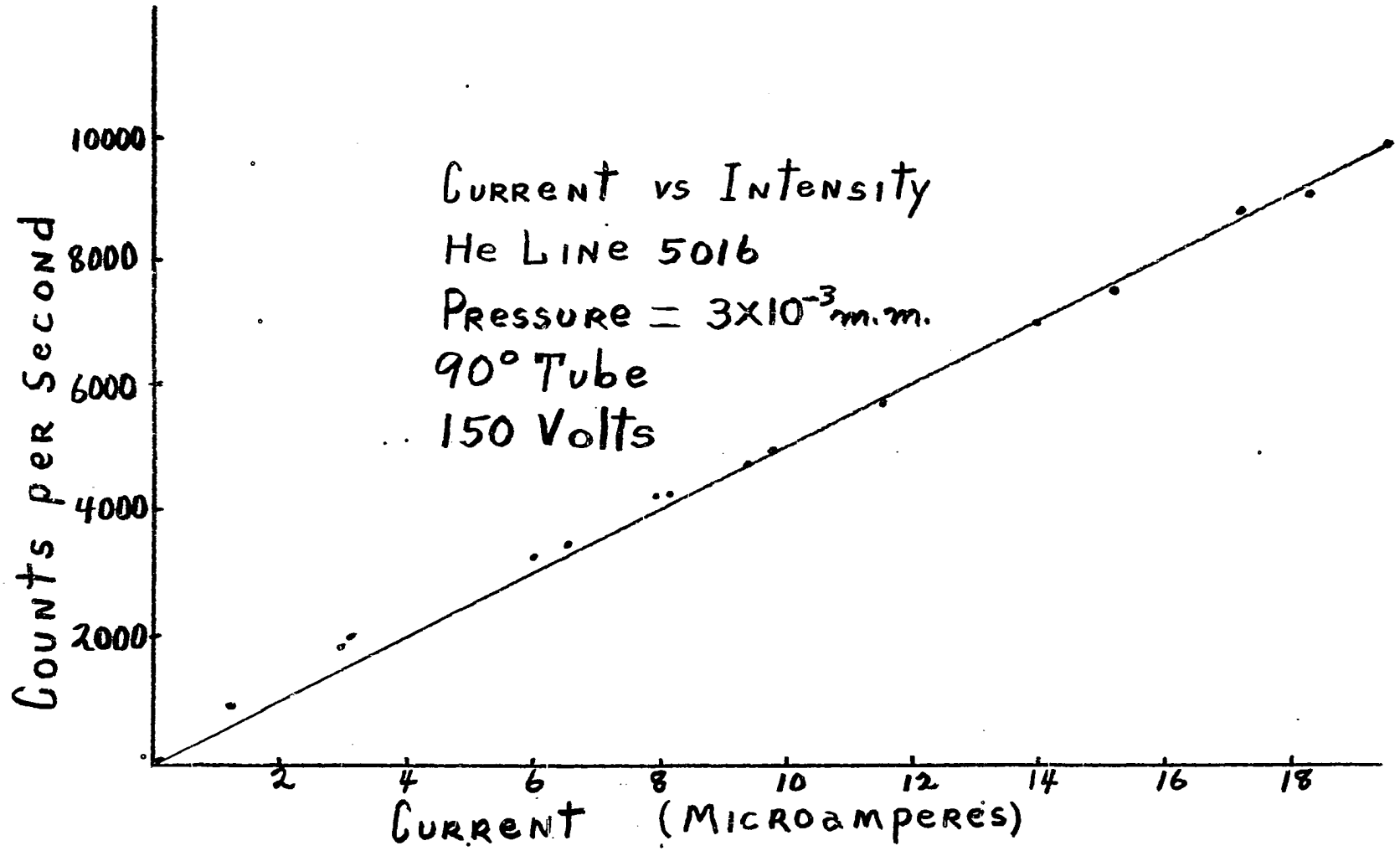

Figure 26. Curve to determine if Multiple Exciting Events Occur

TABLE VI

VARIATION OF COUNT RATE WITH PRESSURE FOR HELIUM LINE 5016A

Taken with: Voltage = 225 Volts
90 Degree Tube

Pressure	Count per Second /μA
$6. \times 10^{-5}$	16.5
2.37×10^{-4}	57.
2.37×10^{-4}	66.3
2.97×10^{-4}	71.1
3.1×10^{-4}	82.1
4.22×10^{-4}	82.2
8.45×10^{-4}	79.4
1.50×10^{-3}	109.
2.2×10^{-3}	145.
2.26×10^{-3}	110.
3.05×10^{-3}	226.
3.82×10^{-3}	148.
3.85×10^{-3}	320.
5.0×10^{-3}	291.
5.65×10^{-3}	450.
5.95×10^{-3}	548.
7.95×10^{-3}	654.
1.5×10^{-2}	1730.
1.52×10^{-2}	2040.
2.25×10^{-2}	3820.
3.30×10^{-2}	8450.

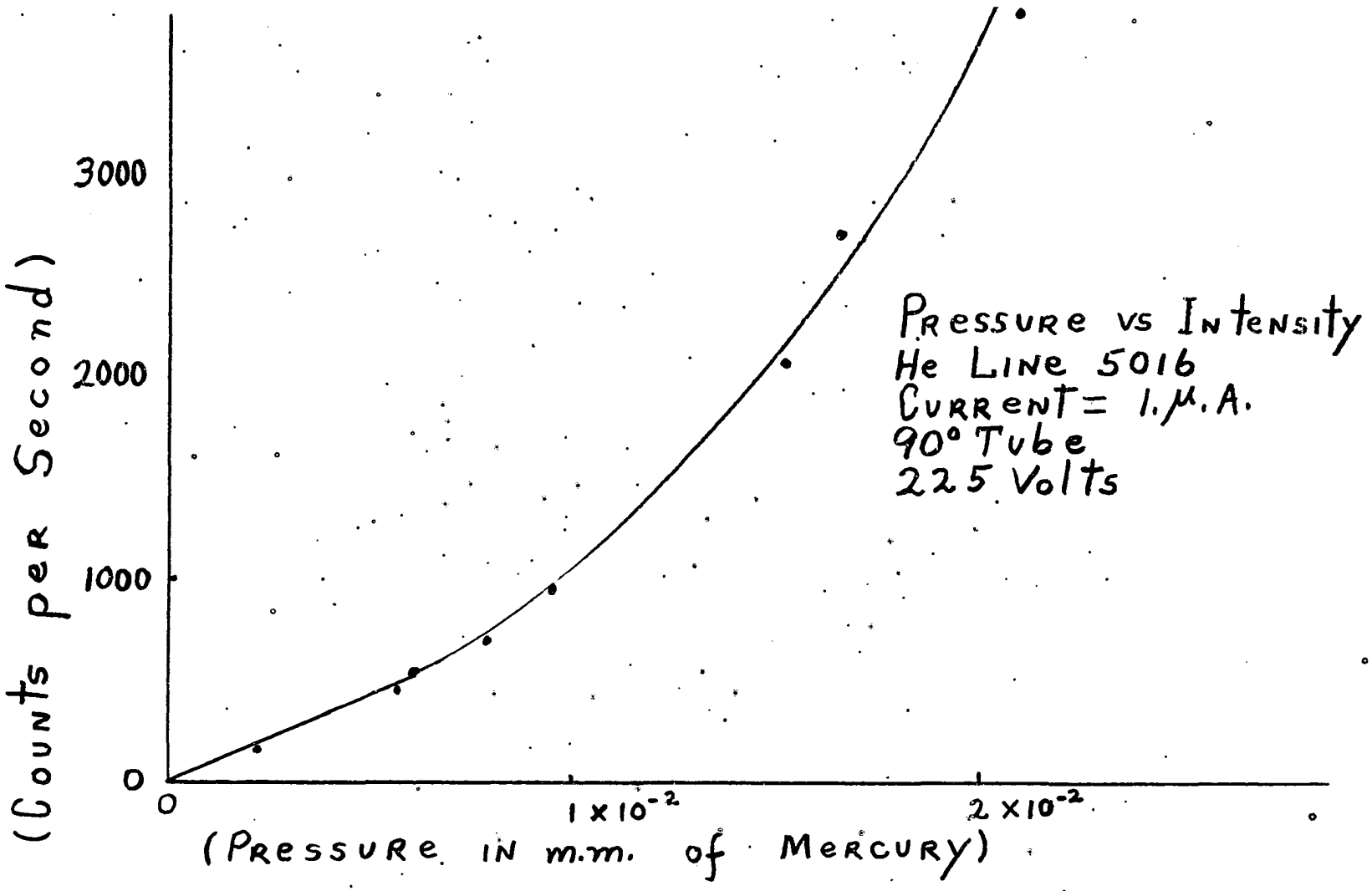

Figure 27. Pressure Versus Intensity for 90° Tube

CHAPTER VIII

EXCITATION CROSS-SECTION VERSUS ELECTRON ENERGY

Calculation of the Cross-Sections From the Observed Data

The absolute magnitude of the excitation cross-section can be calculated when the number of photons of a given wavelength from the excited beam is counted. The light counting efficiency ratio, measured by methods discussed in the preceding chapter, can then be used to convert these relative intensities to absolute ones.

The cross-section (when only first order effects occur, such as an electron exciting one atom only, and when cascading effects are neglected) is defined by the equation,

$$BN_p = I_n N Q_L E d$$

where:

B = branching factor

N_p = number of photons counted per second.

I_n = number of electrons passing a point in the chamber per second.

N = number of gas atoms per centimeter.

Q_L = cross-section for excitation to the L-level from the ground state.

E = fraction of photons emitted from the collision chamber that are counted.

d = length of collision chamber.

Line Factor

The count rates in Figure 28 can be converted into excitation cross-sections for the 3^1P state by multipling them by the line factor. The line factor is defined by the equation,

$$Q_L = N_p L$$

where:

L = line factor.

From the preceding equation, it is seen to be equal to,

$$L = B/I_n N E d.$$

For the 5016A line of helium, for a current of one microampere and a pressure of 5×10^{-3} mm Hg, the line factor was calculated to be $8. \times 10^{-22}$ square centimeters per second per count.

Excitation Function

Figure 28 shows the count rate versus electron energy in electron volts. It can be seen from the slope that the cross-section rises slowly to a maximum value at approximately 65 ev. The peak seems to be some what sharper than was previously reported. Thereafter the curve seems to decrease gradually until it had decreased to about 65 per cent of its peak value at 140 ev.

Figure 29 shows the complete excitation function for the 3^1P state of helium for all electron energies up to 140. ev. The dashed part of the curve represents an extrapolation from the lowest electron energy point measured to threshold. This is the same curve as Figure 28 except the value for the 3^1P cross-section can be read directly from the ordinate and the extrapolation to the threshold is shown.

The high beam energy resolution was not taken advantage of in

making this curve, as this graph was only intended to be a course outline. To obtain a curve with fine resolution many closely spaced points would be needed. Some of these points would need to be spaced .1 volts apart to utilize all the available beam resolution. The main reason for the above coarse plot was to prove the method and get a general outline of the excitation function.

The maximum cross-section for the 3^1P state was measured to be 4.8×10^{-19} square centimeters. This was two orders of magnitude lower than previous experiments. This also agrees much better with the predicted value (14).

During the period of the measurements for the above graph, the sensitivity of the light measuring apparatus showed signs of fluctuating slightly. These fluctuations seemed to accumulate gradually to a maximum of about 10 per cent over a ten minute period. Since the measurements were usually about an hour duration, a check had to be kept on the sensitivity drift. This could have the effect of shifting the maximum in the above curve. It is believed the relative measurements are not off by more than 5 per cent. The equipment is now in the process of being corrected and it is hoped the data taken in the future will not have this dependency.

TABLE VII

DATA TAKEN FOR EXCITATION FUNCTION

Taken with: Pressure = $7. \times 10^{-3}$

Voltage (volts)	Counts per Second per μA
150	380
140	399
130	403
120	416
110	423
100	445
100	390
90	416
80	468
75	536
75	574
70	552
70	557
65	623
65	642
60	572
55	435

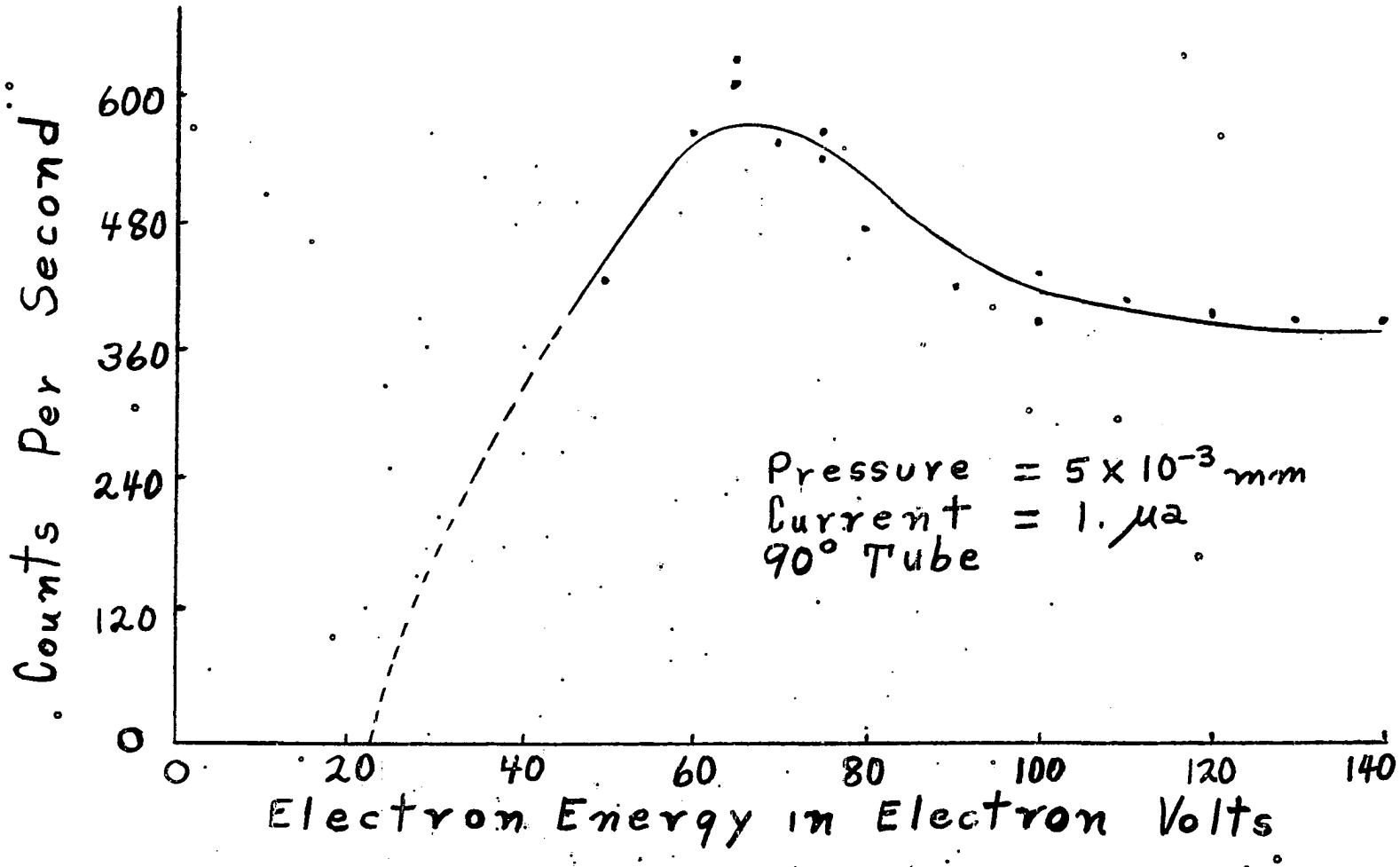

Figure 28. Optical Excitation Function for the 5016A Line of Helium

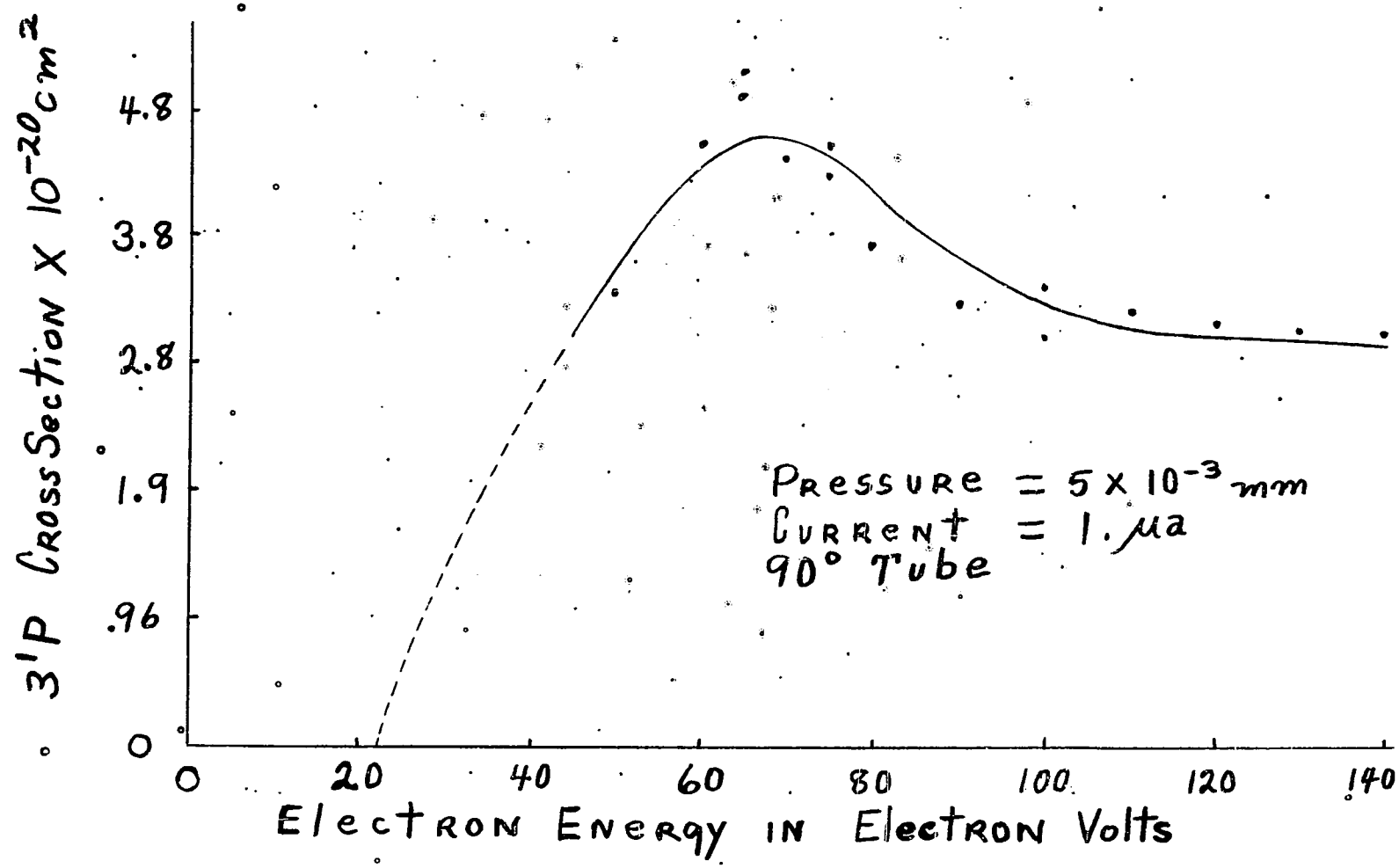

Figure 29. Complete View of the Optical Excitation Function for the 3'P State of Helium

CHAPTER IX

CRITIQUE AND SUMMARY

Work on excitation cross-sections during the period from 1928 to 1934 was carried out to the limit of experimental technique available at the time. A few years later interest was distracted toward nuclear phenomena. The work left many unexplained disagreements and peculiarities. There were disagreements among the various experimental values for the shape and magnitude of the excitation function. There was also disagreement of theory with experiment. One peculiarity (of the experimental work) was the excitation cross section becoming zero for some lines at pressures as large as 10^{-2}mm Hg.

The method described in this thesis was designed around recent advances in experimental technique. The gain in sensitivity attained allows the cross-section to be studied at lower pressures and currents. Because of its great sensitivity, part of the available beam current could be sacrificed leaving a more nearly monoenergetic beam. Velocity resolution was designed for 0.1 ev. This resolution was not needed for the data on the line 5016A presented in this thesis but can be used later to make a study of the excitation function using better resolution.

Although some previous experimenters did not attain linearity in the intensity versus current graphs, it was thought by some that linearity means an electron on the average excites only one atom before it is

collected. Also this is taken to mean that a negligible part of the beam is lost to ionization, elastic scattering etc. during the time it crosses the viewing chamber. Although the author is not certain of the correctness of the above assumption, linearity was observed for the data in Chapter VII.

Lees reported the intensity versus pressure graph for the 5016A line of helium to be linear and intersect the pressure axis at finite pressures. Fowler and Duffendack (6) showed the pressure versus intensity curve to be nonlinear in this region for the helium line 5016A and from indications of its slope to intersect the pressure axis at the origin. They also attained the upper linear region predicted by the Westinghouse group. It seemed to occur at about 1.2mm Hg.

In Lees' photographic experiment, light was observed to be coming from outside the limits of the beam for some lines which seemed to indicate some kind of diffusion process. In the present experiment on the line 5016A, which was one of the lines for which Lees observed the light diffusion, the pressure versus intensity plot showed a non-linearity for pressures down to 5×10^{-3}mm and linearity for further reductions of the pressure. Future measurements will be made at higher pressures to see if the upper linear region predicted by the Westinghouse group can be observed. Although the general shape of the pressure versus intensity curve followed that predicted by Westinghouse in the regions measured, the on-set of the lower linear region (5×10^{-3}mm) was observed to be about five times that predicted (10^{-3}mm).

The magnitude of the maximum excitation function of the helium line 5016A was measured to be 1.2×10^{-20} square centimeters, which is

about two orders of magnitude lower than that measured by Lees and Thieme. The magnitude for the maximum cross-section for the 3^1P state was calculated to be 4.8×10^{-19} square centimeters.

The calculated values according to Born's approximation, which would be expected to give an over estimate, is $2.6 \times 10^{-18} cm^2$. This value predicted by the Born approximation is roughly five times the value of this thesis. The values measured by Lees and Thieme were $3.4 \times 10^{-17} cm^2$ for the maximum cross section of the 3^1P state.

The magnitude for the maximum excitation cross-section obtained by methods of this thesis can be compared with still another way of estimating the maximum excitation cross-section. Corrigan and Von Engel have performed an analysis on recent experimental studies of energy losses of monoenergetic electron beams in helium together with published theoretical excitation functions (4). Their analysis has estimated the cross-section for the 3^1P state up to 30 ev. From an extrapolation of their curve the maximum cross-section is roughly $2.0 \times 10^{-18} cm^2$. This is about four times larger than the result of this thesis. The cross-section for the 3^1P state measured in the present experiment increases slowly with increasing electron beam energy from threshold to a maximum at 65 volts. This is also in agreement with the theory of Corrigan and Von Engel (4).

The value for the maximum excitation cross-section, obtained by the method of this thesis, may be lower than those observed by photographic methods due to the different means used to make the relative intensity measurements absolute.

Excitation cross-sections find applications in understanding pro-

cesses which occur in gaseous discharges, the sun's corona, aurora borelis, gaseous nebula, atomic physics, etc.

BIBLIOGRAPHY

Articles

(1) Alpert, D. "New Developments in the Production and Measurement of Ultra High Vacuum," Journal of Applied Physics, XXIV (1953), 860.

(2) Bates, D.R. and Damgaard, A. "The Calculation of the Absolute Strengths of Spectral Lines," Philosophical Transactions of the Royal Society A,CCXLII (1949), 101.

(3) Born, M. "Quantenmechanik der Stossvorgänge," Zeitschrift fur Physik XXXVIII (1926), 803.

(4) Corrigan, S.J.B. and Von Engel, A. "The Excitation of Helium by Electrons of Low Energy," Proceedings of the Physical Society, LXXII (1958), 786.

(5) Engstrom, R.W. "Multiplier phototube characteristics: Application to Low Light Levels," Journal of the Optical Society XXVII (1947), 420.

(6) Fowler, R.G. and Duffendack, O.S. "Radiative Processes in Thermionically Controlled Discharges in Helium," Physical Review, LXXVI (1949), 81.

(7) Frost, L.S. and Phelps, A.V. "Excitation Functions and Rates for the Principal Levels in Helium," Westinghouse Research Report 6-94439-6-R3 (1957).

(8) Hanle, W. "Messung von Anregungsfunktionen in Heliumspektrum," Zeitschrift fur physik, LVI (1929), 94.

(9) Heron, R.W., McWheeler, Rhoderick "Measurements of Lifetimes of Excited States of Helium Atoms," Proceedings of the Royal Society of London A, CCXXXIV (1956), 565.

(10) Hughes, A. and Lowe, P. "Intensities in Helium Spectrum," Proceedings of the Royal Society of London A, CIV (1923), 480.

(11) Hylleraas, E. "Theoretische Berechnung von Übergangswahrscheinlichkeiten," Zeitschrift fur Physik, CVI (1937), 395.

(12) Lees, J.H. "Excitation Function of Helium," Proceedings of the Royal Society of London A, CXXXVII (1932), 173.

(13) Maier-Leibnitz, H. "Ausbeutemessungen beim Stoss langsamer Elektronen mit Edelgasatomen," Zeitschrift fur Physik, XCV (1935), 499.

(14) Massey, H.S.W. "Theory of Atomic Collisions," Encyclopedia of Physics, XXXVI (1956), 278, 327.

(15) Michels, W.C. "The Optical Excitation Function of Helium," Physical Review, XXXVI (1930), 1362.

(16) Oppenheimer, J.R. "On the Quantum Theory of Electronic Impacts," Physical Review, XXXII (1928), 361.

(17) Phelps, A.V. "Resonance Radiation," Physical Review, CX (1958), 1362.

(18) Peteri, M.G. and Elenbaas, W. "Intensitäten im He-Spektrum als Funktion von Druck und Elektronengeschwindigkeit," Zeitschrift fur Physik, LIV (1929), 92.

(19) Ramsauer, C. "Über den Wirkungsquerschnitt der Gegenuber Langsamen Elektronen," Annulen der Physik, LIV (1921), 513.

(20) Skinner, H.W.B. and Appleyard, E.T.S. "On the Excitation of Polarized Light by Electron Impact," Proceedings of the Royal Society of London, CXVII (1928), 224.

(21) Thieme, O. "Lichtausbeute im Helium -, Quecksilber - und Stickstoff - Spektrum bei Anregung durch Elektronenstoss," Zeitschrift fur Physik, LXXVIII (1932), 412.

Books

(22) Burhop, E.H.S. and Massey, H.S.W. Electronic and Ionic Impact Phenomena. Oxford: Clarendon Press, 1952.

(23) Harwell, G.P. Principles of Electricity and Electromagnetism. New York: McGraw-Hill, 1949.

(24) Mott, N.F. and Massey, H.S.W. The Theory of Atomic Collisions. Oxford: Clarendon Press, (1949).

(25) Schiff, L.I. Quantum Mechanics. New York: McGraw-Hill, (1949) 159.